
Doctoral Dissertations

Student Theses and Dissertations

Summer 2019

High level thermochemical and spectroscopic computations for molecules relevant to combustion and the atmosphere

Bradley K. Welch

Follow this and additional works at: https://scholarsmine.mst.edu/doctoral_dissertations

 Part of the [Physical Chemistry Commons](#)

Department: Chemistry

Recommended Citation

Welch, Bradley K., "High level thermochemical and spectroscopic computations for molecules relevant to combustion and the atmosphere" (2019). *Doctoral Dissertations*. 2814.
https://scholarsmine.mst.edu/doctoral_dissertations/2814

This thesis is brought to you by Scholars' Mine, a service of the Missouri S&T Library and Learning Resources. This work is protected by U. S. Copyright Law. Unauthorized use including reproduction for redistribution requires the permission of the copyright holder. For more information, please contact scholarsmine@mst.edu.

HIGH LEVEL THERMOCHEMICAL AND SPECTROSCOPIC COMPUTATIONS
FOR MOLECULES RELEVANT TO COMBUSTION AND THE ATMOSPHERE

by

BRADLEY KENNETH WELCH

A DISSERTATION

Presented to the Faculty of the Graduate School of the
MISSOURI UNIVERSITY OF SCIENCE AND TECHNOLOGY

In Partial Fulfillment of the Requirements for the Degree

DOCTOR OF PHILOSOPHY

in

CHEMISTRY

2019

Approved by:

Richard Dawes, Advisor
Philip Whitefield
Paul Parris
Garry S. Grubbs
Jeffrey Winiarz

© 2019

Bradley Kenneth Welch

All Rights Reserved

PUBLICATION DISSERTATION OPTION

This dissertation consists of the following two articles, formatted in the style used by the Missouri University of Science and Technology:

Paper I: Pages 7-25 have been accepted by Journal of Molecular Structure.

Paper II: Pages 26-52 are submitted to Journal of Physical Chemistry A.

ABSTRACT

Computational thermochemistry can be a complicated multistep process, but in recent years has become an equal partner with experiment. Many important molecules in combustion systems or in the atmosphere (such as short-lived radicals) are difficult to study experimentally. Predicting highly accurate thermochemistry is a key aspect in understanding these species. In this project, computational thermochemistry was developed into an automated streamlined procedure and then used to understand the methyl and ethyl peroxy families of radicals. This effort involved optimizing a standard workflow for computational thermochemistry. Computational thermochemistry generally requires numerous individual calculations whose cost and scalings vary widely. Conducting such tedious procedures manually can easily introduce errors. Here, a multifunctional code called EXATHERM was developed. A first generation with fixed procedures was implemented as a proof of principle and then a second generation that is more flexible was implemented via the module formalism of Python.

ACKNOWLEDGMENTS

First I would like to thank Dr. Richard Dawes. He introduced me to the world of highly accurate thermochemistry as well as provided useful advice during the span of my project. He also helped in the preparation of my SCGSR Fellowship which exposed me to the national laboratory environment. I would also like to thank Drs Branko Ruscic and David Bross. Both provided guidance during my time at Argonne National Laboratories. Without them I would not have learned as much as I did about highly accurate thermochemistry and the Active Thermochemical Tables.

I would also like to thank my fiancé Kelsey for giving me much encouragement during my time in graduate school. I would also like to thank my mom for being there.

I would also like to thank the supergroup I worked with for 4 years. Stephen, Ernesto, and Sangeeta thanks for the fun times at ISMS as well as the useful discussions about everything.

TABLE OF CONTENTS

	Page
PUBLICATION DISSERTATION OPTION	iii
ABSTRACT.....	iv
ACKNOWLEDGMENTS	v
LIST OF ILLUSTRATIONS.....	ix
LIST OF TABLES.....	x
 SECTION	
1. INTRODUCTION.....	1
1.1. THERMOCHEMISTRY	1
1.2. ACTIVE THERMOCHEMICAL TABLES.....	3
1.3. AUTOMATION	5
 PAPER	
I. REACTIVE PATHWAYS IN THE BROMOBENZENE-AMMONIA DIMER CATION RADICAL: EVIDENCE FOR A ROAMING HALOGEN RADICAL	7
ABSTRACT.....	7
1. INTRODUCTION.....	8
2. EXPERIMENTAL AND COMPUTATIONAL DETAILS	10
3. RESULTS AND DISCUSSION	11
4. CONCLUSIONS	21
REFERENCES.....	21

II. AN AUTOMATED THERMOCHEMISTRY PROTOCOL BASED ON EXPLICIT-CORRELATED COUPLED-CLUSTER THEORY: THE METHYL PEROXY FAMILY.....	26
ABSTRACT	26
1.INTRODUCTION.....	27
2.COMPUTATIONAL DETAILS	29
3.RESULTS AND DISCUSSION	34
3.1 METHYLPEROXY RADICAL	35
3.2. METHOXYOXONIUMYLIDENE (METHYL PEROXY CATION)	37
3.3. METHYL HYDROPEROXIDE.....	38
3.4. METHYLPEROXY ANION	39
3.5. ETHYLPEROXY RADICAL	39
3.6. ETHYL HYDROPEROXIDE	42
3.7. ETHYLPEROXY ANION	43
4. CONCLUSION	43
ACKNOWLEDGEMENT.....	44
REFERENCES	45
SECTION	
2. CONCLUSIONS	53
APPENDICES	
A. SUPPORTING INFORMATION FOR PAPER I.....	54

B. SUPPORTING INFORMATION FOR PAPER II.....	64
C. USER GUIDE TO EXATHERM V.1	72
BIBLIOGRAPHY.....	78
VITA.....	80

LIST OF ILLUSTRATIONS

SECTION	Page
Figure 1.1. Uncertainties of different determinations of CH_3 comparing Gurvich, JANAF, and ATcT	4
PAPER I	
Figure 1. Time-of-flight mass spectrum obtained following two-step ionization at a wavelength of 269.5 nm. The two observed peaks in this region correspond to aniline cation radical and protonated aniline, as shown.....	13
Figure 2. Upper panel: comparison of R2PI spectra of the PhBr monomer and PhBr-NH ₃ complex. The latter spectrum was obtained by monitoring the protonated aniline mass channel. Lower panel: trend in the blue-shift of the dimer excitation spectrum for PhX-NH ₃ dimers (X=F, Cl, Br), data taken from refs. 26 and 27.	14
Figure 3. Upper panel: calculated stationary points on the cation radical surface of the PhCl···NH ₃ system. Lower panel: similar calculations for the PhBr···NH ₃ dimer.	17
Figure 4. Contour plot of the interaction between the roaming Br-atom and the Ph-NH ₃ fragment. Labeled contours indicate the energy in kJ/mol and illustrate the attractiveness of the NH ₃ protons to the roaming Br-atom.....	20
PAPER II	
Figure 1. Flowchart of the automated thermochemical protocol. Details of each contribution to the composite energy and the pre- and post-processing procedures are given in the text.	31
Figure 2. Some relevant structural parameters for members of the methyl peroxy family (distances in Angstroms and angles in degrees). CH ₃ O ₂ structures b), c) and d) are those of the neutral radical, cation, and anion systems respectively.	36
Figure 3. Some relevant structural parameters of the Ethyl Peroxy and Hydroperoxide species. a.) being the radical, b.) the anion, and c.)the hydroperoxide species.	40

LIST OF TABLES

PAPER I	Page
Table 1. Parameters used in microcanonical TS calculations for the Br atom loss and HBr atom loss channels.....	19

1. INTRODUCTION

1.1. THERMOCHEMISTRY

Highly accurate thermochemistry is essential to understanding chemical processes and advancing chemical industries. Accurate thermochemistry is key to understanding kinetic processes, spectroscopy, as well as the possible channels a reaction can explore.¹ Inaccurate thermochemistry can lead to inaccurate predicted rate constants which leads to a poor understanding of the relevant kinetics. Even a 1 kJ/mol error in an enthalpy of reaction can lead to an incorrect rate constant due to the exponential nature of the Arrhenius equation.

Accurate computational thermochemistry has only recently become routine. While computational thermochemistry is not a new field,² accurate computational thermochemistry is only a recent phenomenon. The HEAT method demonstrated that achieving the sub-chemical level of accuracy (>1 kJ/mol) was doable.³ The Wn methods of Martin followed.^{4,5,6} Now there are multiple “highly-accurate” thermochemical schemes. Obtaining subchemical accuracy is still a challenge and only possible for small systems. Obtaining “chemical accuracy” of >4 kJ/mol on the other hand is now practical for medium sized molecules.⁷ A common theme in all of these thermochemical methods is that they assume that an accurate electronic energy can be obtained by a composite approach as shown in equation 1:

$$\Delta E = \Delta E_{\text{HF}} + \Delta E_{\text{coupled cluster}} + \Delta E_{\text{CV}} + \Delta E_{\text{ZPVE}} + \Delta E_{\text{HOC}} + \Delta E_{\text{SO+Rel}} + \Delta E_{\text{DBOC}}, \quad (1)$$

where ΔE_{HF} is the Hartree-Fock energy, $\Delta E_{\text{coupled cluster}}$ is the coupled cluster energy. Often in high accuracy computational thermochemistry the CCSD and (T) energies are of the

extrapolated separately. ΔE_{CV} is the energy of the core electrons. ΔE_{ZPVE} is the gap between the bottom of the well and first vibrational level *i.e.* the zero point energy. Due to the fact that molecular vibrations are not harmonic, then this term is typically either scaled by an empirical factor,⁸ or in a more rigorous approach, the anharmonic zero point energy is computed. In practice, this can be accomplished by computing the harmonic frequencies with a high quality method, and using a cheaper method for the anharmonic portion.⁹⁻¹⁰ ΔE_{HOC} denotes higher order correlation beyond CCSD(T). In most cases it is estimated via CCSDT and CCSDT(Q). ΔE_{SO+Rel} is the spin-orbit contribution and a correction for relativistic effects. Spin-Orbit is most often only included for atomic species.⁹ While relativistic effects are only a small contributor to the total energy of a 1st row molecule, for second row elements and beyond, this effect can grow to become a vitally large contributor, and as such, in general it should be computed due to the ease of doing so, and its availability in multiple computational packages.⁶ Finally, the last term in Eq. 1, ΔE_{DBOC} is the Diagonal Born Oppenheimer Correction, a 1st order correction for the Born-Oppenheimer assumption.¹¹ The geometry used for these computations is often one optimized with CCSD(T) and a medium to large sized basis set.^{3,5-6}

The overall cost of the composite procedure given in Eq. 1 can be prohibitive. One avenue to limit costs is to compute the coupled cluster valence energy and core valence components via explicitly correlated coupled cluster theory (known as F12).¹² F12 methods greatly accelerate complete basis set (CBS) extrapolation and thus provide better converged results at lower cost.¹³ Significantly more accurate results can be obtained with a smaller basis set than conventional coupled cluster theory. Coupled cluster with singles, doubles, and perturbative triples is quite costly scaling as n^7 with the n .¹²⁻¹³ A smaller basis

set used here would reduce resource usage as well as allow for larger molecules to be treated. Another advantage of F12 methods is to permit the use of a smaller basis set for geometry optimization. Even the cc-pvdz-f12 basis set is known to give both excellent geometrical parameters and harmonic frequencies.¹⁴ This is a massive savings in time compared to achieving comparable results using standard CCSD(T). It is also much more accurate than lower level methods like density functional theory, or MP2.

1.2. ACTIVE THERMOCHEMICAL TABLES

Historically thermochemistry has relied upon a linear sequence of experimental and computational determinations. These have been collected in various compilations (CODATA, JANAF, Gervich).¹⁵⁻¹⁷ Often they would not be critically evaluated for what was considered the best thermochemical value.¹⁸ Even if a new determination arose that changed the values related to a core thermochemical species (say water), then this was not used to update other determinations. With the Active Thermochemical Tables (ATcT) this is not the case. The ATcT critically evaluates multiple sources of thermochemical evaluations and uses them to rapidly update all connected enthalpies of formation.¹⁸⁻¹⁹ Remarkably, the globally self-consistent procedure provides the user of the database with an uncertainty for enthalpy of formation that is less than that of any one determination. As seen in Figure 1.1 for the CH₃ species the uncertainty for that species is considerably smaller for ATcT than the other databases (and indeed smaller than any particular contributing measurement or calculation).

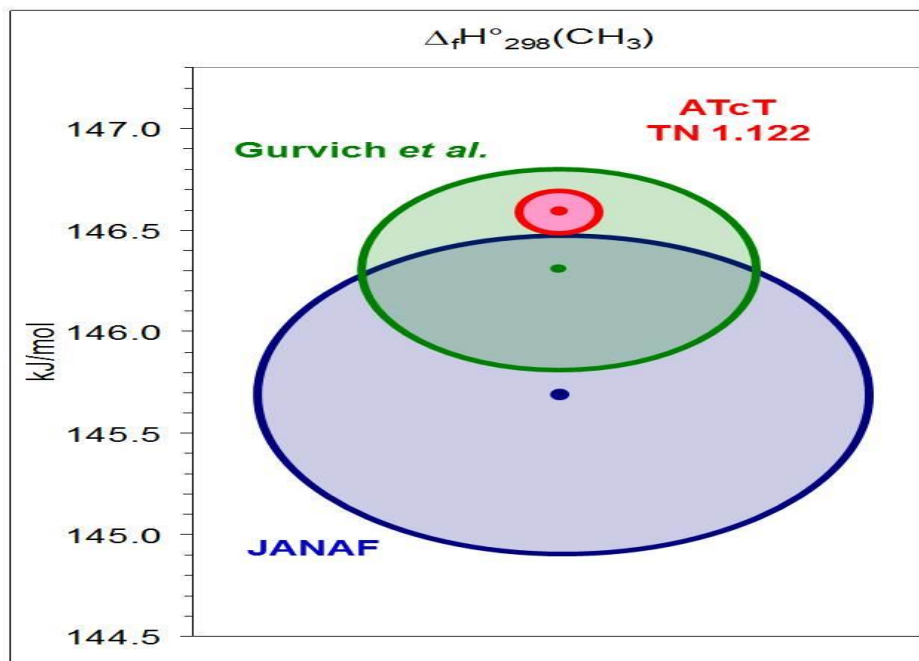


Figure 1.1. Uncertainties of different determinations of CH_3 comparing Gurvich, JANAF, and ATcT

The ATcT procedure is capable of determining outliers and either removing them altogether, or reducing their contribution to the enthalpy of formation. The method can identify weak links in the network and help guide contributors as to which molecules would benefit from additional more accurate determinations.¹⁸⁻²¹ Another area of contribution that has been key is in reanalyzing older determinations. Often in the past, the assigned uncertainty of an experiment was too optimistic.²¹ The ATcT can decide whether the uncertainty is too optimistic and if so, the uncertainty can be reassigned for the offending contributor.²¹

An important aspect of the ATcT is that it can seamlessly use computational values for determining an enthalpy of formation. For many chemical species (short-lived

intermediates in a reaction, certain radicals, and charged species) the only way to obtain information about them is via computational chemistry.²² Many species in the ATcT have a computational contribution, and for some the only contributions are computational. The ATcT also gives computational chemists a highly accurate benchmark to compare with their methods under development due to the small uncertainty of many species in the table.²⁰

1.3. AUTOMATION

Immediately obvious from Eq. 1 and the number of thermochemical recipes in the literature is that computational thermochemistry is a non-trivial task. It requires the use of multiple codes to obtain the single result of a highly accurate energy. The various codes used to compute the different terms all have different input file structures. If manually prepared, this risks introducing mistakes in input, leading either to the codes not running at all, or introducing an error that would lead to erroneous results only spotted during data analysis (if at all). A facet of this work described in Paper 2 was involved in developing a code that not only automatically writes the input files for the separate codes, but also runs them. The code also post-processes the results, collecting the final computed data, and provides the ultimate value of interest, enthalpy of formation. Additional information reported in the output also includes a breakdown of the contribution to the total atomization energy (TAE), as well as their percent contribution. At the bottom of the output is listed the raw electronic energies. These are provided so the researcher can use them when checking what would be the effect of changing procedures.

This leads to a second generation of python code that is more flexible, implemented via modules. This code now only requires the user to provide in the input file which codes the user selects to use, and the basis set for the particular module. This gives the user complete flexibility in terms of all the details of the overall procedure. The weakness of a family of fixed hardwired scripts is that the user might not have access to those specific code packages, or simply might prefer to employ a more suitable procedure in a given case.

PAPER**I. REACTIVE PATHWAYS IN THE BROMOBENZENE-AMMONIA DIMER CATION RADICAL: EVIDENCE FOR A ROAMING HALOGEN RADICAL**

Silver Nyambo¹, Brandon Uhler¹, Lloyd Muzangwa¹, Maxim Ivanov¹, Bradley K. Welch², Richard Dawes², Scott A. Reid¹

¹ Department of Chemistry, Marquette University, P. O. Box 1881, Milwaukee, WI 53201, USA

² Department of Chemistry, Missouri University of Science and Technology, Rolla, MO 65409, USA

ABSTRACT

Photoinitiated reactions in van der Waals complexes provide a means to examine reactive pathways from well-defined initial geometries. In recent work, we re-examined reactive pathways following resonant two-photon ionization (R2PI) of the chlorobenzene-ammonia (PhCl---NH₃) dimer. The dimer cation radical reacts primarily via Cl atom loss and additional channels corresponding to HCl and H atom loss were identified. The structure of the reactive complex was confirmed as an in-plane σ -type, and computational studies of the dimer cation radical potential energy landscape revealed two nearly isoenergetic arenium ion intermediates (or Wheland intermediates). The intermediate produced from *ipso* addition was not stable with respect to either Cl or HCl loss, and the relative branching observed in experiment was well reproduced by microcanonical transition state theory (TST) calculations. Here, we report experimental and computational studies of the related PhBr···NH₃ dimer, examined for the first time. We present evidence that the dimer structure is also an in-plane σ -type. However, in

contrast to the $\text{PhCl}\cdots\text{NH}_3$ system, calculations predict that the structure of the reactive intermediate corresponds to a distonic ion-radical complex, where the radical density is largely localized on the bromine atom. The calculated barrier to HBr loss is sufficiently high to render this channel nearly insignificant (less than 1% branching) in TST calculations, yet experiment shows a sizable (37%) branching into this channel. We rationalize these results in terms of a roaming Br radical mechanism for HBr formation.

1. INTRODUCTION

The study of van der Waals clusters has provided important insight into the strength and directionality of intermolecular forces, and detailed experimental data (binding energies, vibrational and electronic spectra, etc.) on these systems provide important benchmarks for theoretical validation.¹⁻⁸ Additionally, clusters provide a means to initiate reactivity from relatively well-defined initial geometries.⁹⁻¹² Prototypical systems in this regard are the dimers of halobenzenes with ammonia (i.e., $\text{PhX}\cdots\text{NH}_3$) which upon ionization can react via a classic $\text{S}_{\text{N}}2$ mechanism proceeding through an arenium ion (Wheland) intermediate.¹³⁻²⁵ Until recently, it has been thought that the structure of these dimeric complexes were π -type, where the ammonia is located above the plane of the aromatic ring. This was dispelled by studies of the Cockett group²⁶ (on fluorobenzene-ammonia) and our group²⁷ (on chlorobenzene-ammonia), which showed, via multidimensional Franck-Condon simulations of the excitation spectra, that the reactive complex corresponds to an in-plane σ -type.

We recently re-investigated the reactive pathways in the well-studied^{13-18,25,28} chlorobenzene-ammonia dimer cation radical using resonant two-photon ionization

(R2PI) and electronic structure calculations (density functional theory, DFT).²⁷ In addition to the well-studied Cl loss channel (producing protonated aniline),^{13-18,25,28} a second channel corresponding to HCl loss (producing aniline cation radical) was identified for the first time in R2PI studies of the 1:1 complex, and a third channel, H atom loss, was also identified. The reactive potential energy landscape was extensively characterized by computational methods, and two nearly isoenergetic arenium ion (Wheland) intermediates were found. At the energy accessed experimentally, the intermediate produced from *ipso* addition was not stable with respect to Cl or HCl loss, and the relative observed branching between these channels (1:5.6 with Cl loss dominant) was well reproduced by microcanonical transition state theory calculations.

To date, no experimental studies have probed complexes between bromobenzene (PhBr) and ammonia, primarily due to the fact that the S1 lifetime of PhBr is very short (~30 ps)^{29,30} and it is therefore difficult to resonantly ionize with nanosecond lasers.³¹⁻³⁴ Our initial interest in this system stemmed from the possibility of accessing halogen bonded structures. Thus, in the present work, we examine the formation and fate of the ionized complexes of PhBr and NH₃ using one-color R2PI spectroscopy, supported by DFT, time-dependent DFT, and ab initio calculations at the explicitly-correlated coupled-cluster level, as well as Franck-Condon simulations. Consistent with other PhX...NH₃ (X=halogen) dimers, we find that the observed complex is of a σ -type. However, the structure of the ionic intermediate predicted via theory is very different from that in the PhCl...NH₃ system, being a distonic ion-radical complex, where the radical density is largely localized on the Br atom. Calculations predict a sizable barrier to HBr elimination from this intermediate, sufficient to yield very little statistical branching into this channel, yet we

observe a branching for the molecular channel (37%) which is significantly larger than in the analogous $\text{PhCl}\cdots\text{NH}_3$ system (15%). Given the structure of the intermediate, and the lower energy exit channel to Br elimination, we postulate the existence of a roaming radical mechanism to explain the increased yield of the molecular channel.

2. EXPERIMENTAL AND COMPUTATIONAL DETAILS

The experimental setup has previously been described in detail.²⁷ Our R2PI setup comprises a linear time-of-flight mass spectrometer (TOFMS) coupled with a supersonic molecular beam source. The expanded mixture was generated by passing a 1-5% NH_3/He premix through liquid bromobenzene (Aldrich, 99%) contained in a stainless-steel bubbler held at 25°C. The backing pressure was varied between ~2-5 bar. Ions were extracted and accelerated using a conventional three-plate stack, and flew through a 1 m field-free drift region prior to striking a dual Chevron microchannel plate (MCP) detector. The detector signal was amplified (x 20) using a fast preamplifier (Femto HVA-500M-20B), and integrated using a boxcar system (Stanford Research SRS250) interfaced to a personal computer. The laser system consisted of an etalon narrowed dye laser (Lambda Physik Scanmate 2E) pumped by a third harmonic of a Nd:YAG laser (Continuum NY-61). Coumarin 540A was used for the dye laser; its lasing range was ~530-550 nm. The output of the dye laser was then frequency doubled, giving an output wavelength range of 265 to 285 nm. The doubled laser beam of energy range ~ 0.5 mJ was loosely focused into the chamber by a 2 m plano-convex lens. An in-house LABVIEW program controlled data acquisition and stepped the laser wavelength; typically, the signal from twenty laser shots was averaged at each step in wavelength.

Our experimental findings were supported by two types of electronic structure calculations. DFT calculations were performed using the GAUSSIAN09 software package on the MU Pere high speed cluster.³⁵ Geometry optimizations were carried out using the M06-2X method³⁶ with the aug-cc-pVDZ and aug-cc-pVTZ basis sets. The performance of M06-2X for electronic excitations, including Rydberg and Charge Transfer excitations, has recently been benchmarked,³⁷ and performed well on the similar chlorobenzene-ammonia system.²⁷ The MOLPRO package³⁸ was used to perform single-point energy calculations using the explicitly-correlated coupled-cluster (U)CCSD(T)-F12a/VDZ-F12 method.^{39,40} The small-core pseudo-potential (PP) basis by Peterson was used for bromine.⁴¹ Calculated coupled-cluster binding energies were corrected for zero-point energy (ZPE) using DFT. The vertical excitation energies and the electronic spectra of the dimers were calculated by employing Time-dependent DFT (TD-DFT) method at M06-2X/aug-cc-pVDZ level of theory. For the cation radical states, calculations were also performed using a calibrated⁴²⁻⁴⁴ B1LYP functional (B1LYP-40), with a 6-31G(d) basis set. R2PI excitation spectra were simulated by performing multidimensional Franck-Condon calculations using the Pgopher program.⁴⁵

3. RESULTS AND DISCUSSION

In our previous work on the PhCl \cdots NH₃ system, we found that upon ionization the majority of dimer cation radicals reacted, leading to a very small signal in the time-of-flight mass spectrum at the parent mass/charge ratio (m/z). Given the difficulty in ionizing PhBr, and the concomitant decrease in signal, it was not possible to measure an R2PI spectrum on the parent m/z. However, consistent with our prior findings for

PhCl \cdots NH₃, a strong signal could be detected in the aniline cation radical and protonated aniline channels, as shown in Figure 1, indicative of HBr and Br loss, respectively, from an ionized precursor. We provide evidence below that this signal arises from the ionized PhBr \cdots NH₃ dimer.

The R2PI spectrum obtained by scanning the excitation laser while integrating the signal over the protonated aniline mass channel is compared with the bromobenzene R2PI spectrum in the upper panel of Figure 2. The spectrum is similar to that observed for the PhCl \cdots NH₃ dimer in: 1) the appearance of an origin blue-shifted from the monomer, and 2) a strongly diagonal transition exhibiting little vibronic activity. Moreover, the magnitude of the blue-shift from the monomer origin follows the trend observed for the PhF \cdots NH₃ and PhCl \cdots NH₃ dimers, as shown in the lower panel of Figure 2. This data provides strong evidence that the species responsible for the mass peaks observed in Figure 1 is a π -type PhBr \cdots NH₃ dimer.

Additional evidence is provided by theory. Initial geometry optimizations at the M06-2X/aug-cc-pVTZ level identified four minima, with structures shown in Figure A1 in appendix . These correspond to two in-plane σ -type complexes (D1, D2), a halogen bonded complex (D3), and a π -type complex (D4). At this level of theory, the calculated binding energies, counterpoise and ZPE corrected, of D1 and D4 are similar, \sim 6.5 kJ/mol, while the halogen bonded dimer D3 is bound by 3.7 kJ/mol, and D2 by 2.9 kJ/mol. However, binding energies at the explicitly-correlated coupled-cluster level are significantly different, and clearly favor D1. At the CCSD(T)-F12a/VDZ-F12 level (with M06-2X ZPE corrections), the binding energies are: 8.38, 4.25, 5.98, and 5.99 kJ/mol for structures D1-D4 respectively.

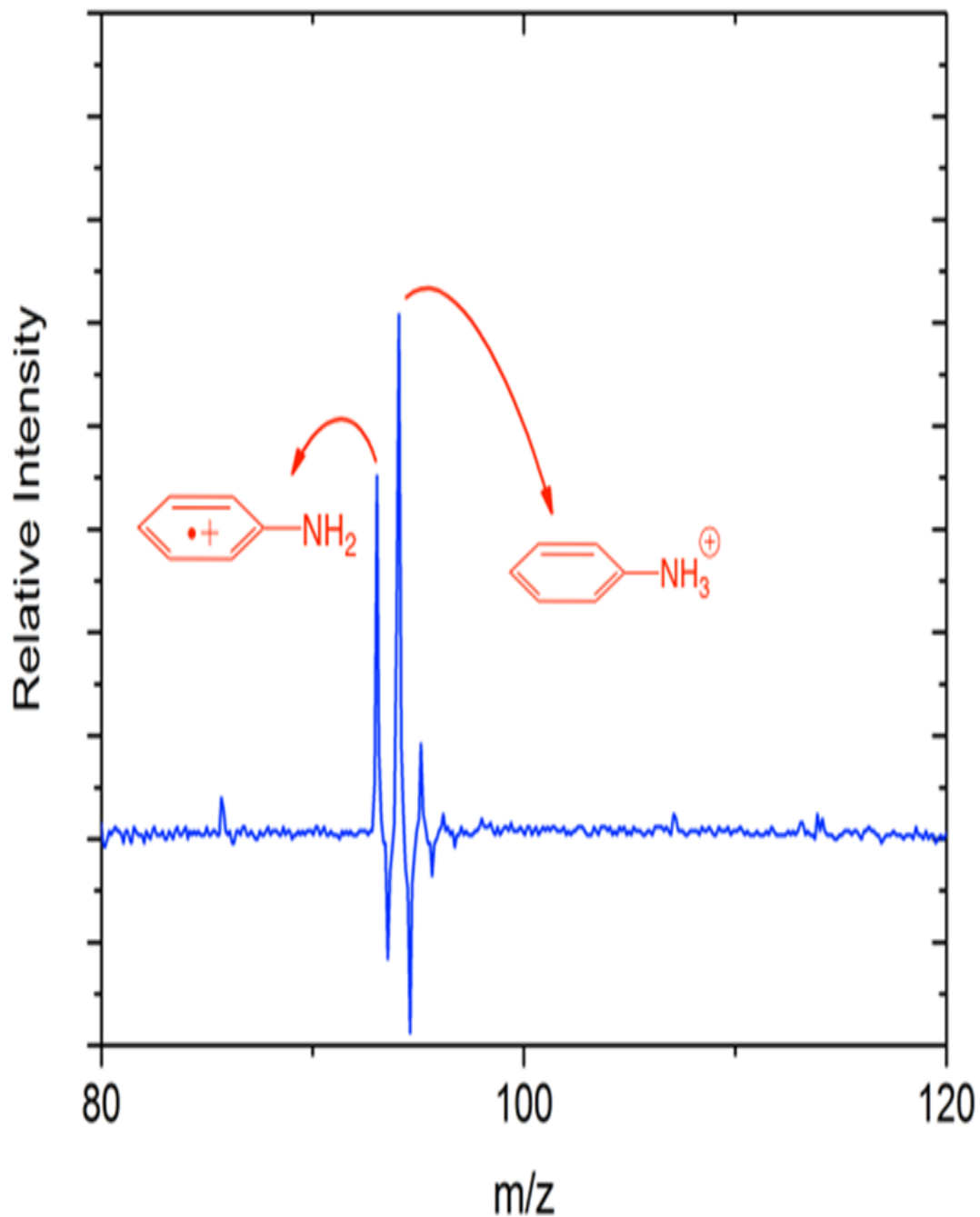


Figure 1. Time-of-flight mass spectrum obtained following two-step ionization at a wavelength of 269.5 nm. The two observed peaks in this region correspond to aniline cation radical and protonated aniline, as shown.

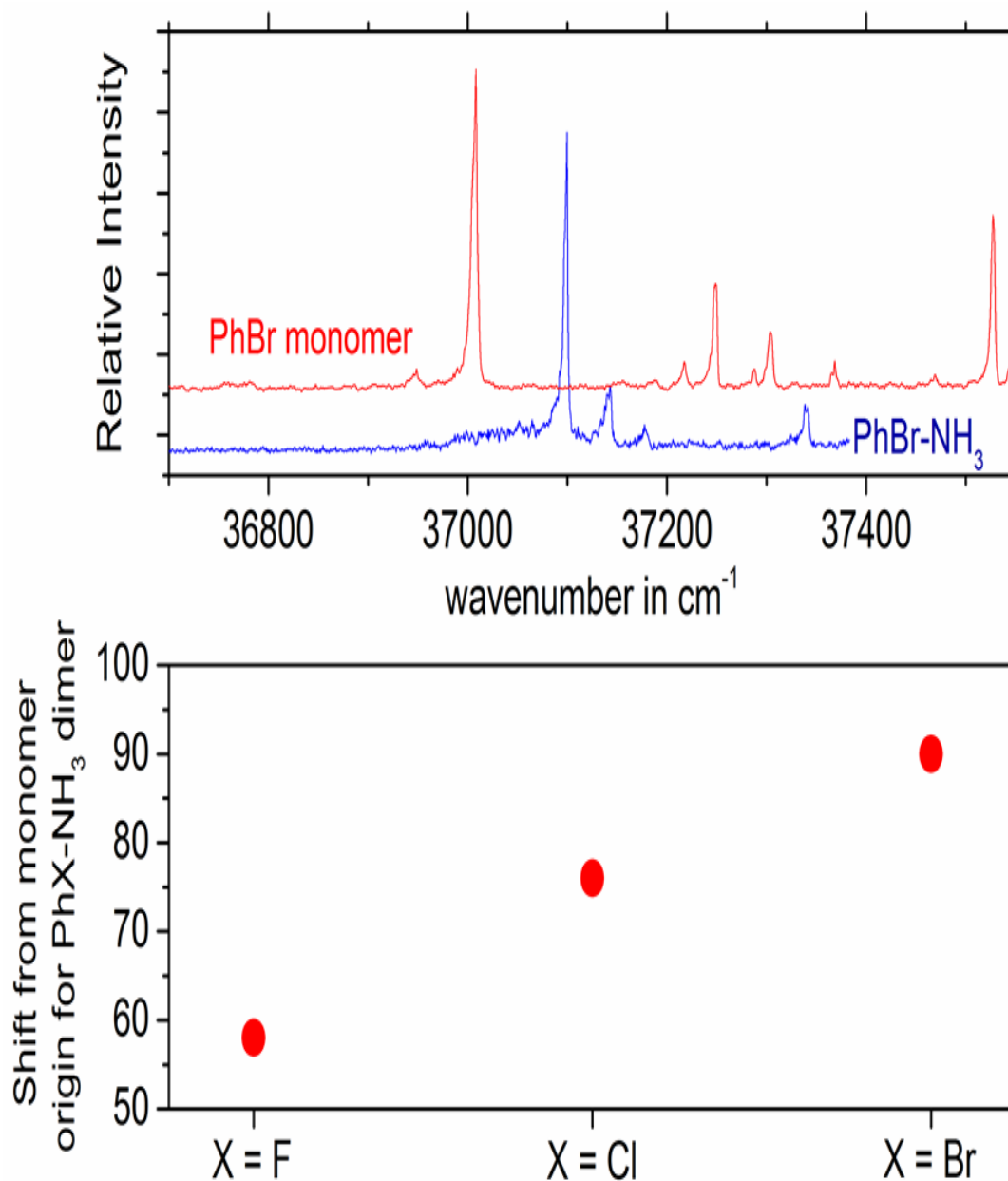


Figure 2. Upper panel: comparison of R2PI spectra of the PhBr monomer and PhBr-NH₃ complex. The latter spectrum was obtained by monitoring the protonated aniline mass channel. Lower panel: trend in the blue-shift of the dimer excitation spectrum for PhX-NH₃ dimers (X=F, Cl, Br), data taken from refs. 26 and 27.

As shown in Figure A2 in appendix, TDDFT calculations predict a blue-shift of the dimer origin for the σ -type complex D1 relative to the PhBr monomer, while the π -type complex (D4) is predicted to show a small red-shift.

Indeed, when scaled to the experimental transition energy, the magnitude of the blue shift for D1 is in good agreement with experiment (Figure A2), as was also found for the PhCl \cdots NH₃ dimer.²⁷ Thus, the position of the observed origin is also consistent with assignment to the σ -type complex D1.

Further evidence comes from Franck-Condon simulations, based upon the optimized geometries, vibrational frequencies, and mass-weighted normal mode displacements for the ground and excited states, incorporating the full effect of Duschinsky rotation.⁴⁶ These calculations, carried out with the Pgopher suite,⁴⁵ were performed for the σ -type complex D1 and the π -type conformer (D4), and only the lowest frequency modes (maximum of 5) were included in the simulation. Figure A3 in appendix shows the simulated electronic spectra with an overlay of the experimental spectrum. Stick spectra were transformed into continuous spectra by convolution with a Gaussian function of 5 cm⁻¹ full width at half-maximum. The simulation for the π -type (D4) isomer shows extended Franck-Condon progression, arising from the significant change in equilibrium geometry from the ground to the excited state, and is in direct contrast with the origin-dominated experimental spectrum. However, the simulated spectrum of the σ -type (D1) complex well matches the experimental spectrum, providing additional support for assignment of the observed electronic spectrum to the σ -type complex D1.

Having reasonably established the structure of the dimer, we now turn to the reactive pathways operative upon ionization. Based upon our prior findings for the PhCl \cdots NH $_3$ dimer,²⁷ shown in Figure 3(a), we believed that the cation radical PES should feature an arenium ion (Wheland) intermediate produced from *ipso* addition, which would react to yield both atomic and molecular products. However, the calculated stationary points for the ionized PhBr \cdots NH $_3$ dimer, Figure 3(b), are strikingly different. The intermediate produced from *ipso* addition does not correspond to a classic Wheland structure; rather, it is a distonic ion-radical complex of protonated aniline and a bromine atom. The latter is pushed quite far from the aromatic ring, so that the distance to the *ipso* carbon (3.30 Å) is significantly larger than the distance to the nearest amino hydrogen (2.53 Å); Figure A4. Calculations at the B1LYP-40/6-31G(d) level reveal that the radical density is largely localized on the bromine atom, Figure A5.

This change in intermediate structure leads to manifest differences in the resulting decay pathways, i.e., compare Figure 3(a) and 3(b). Halogen atom elimination is barrierless (Figure 3(b)), and the barrier for hydrogen halide elimination is significantly increased in comparison with the PhCl \cdots NH $_3$ system. Similar to the dimer calculations, the energies plotted in Figure 3 were obtained as single-point UCCSD(T)-F12a/VDZ-F12 energies, ZPE corrected at the M06-2X/aug-cc-pVTZ level. Additional data from the DFT calculations are provided in the supporting information (Figures A6 and A7). As a further check, we also performed a full optimization of the distonic intermediate at the CCSD/aug-cc-pVTZ level (Figure A8). The structure is similar to that obtained with DFT methods.

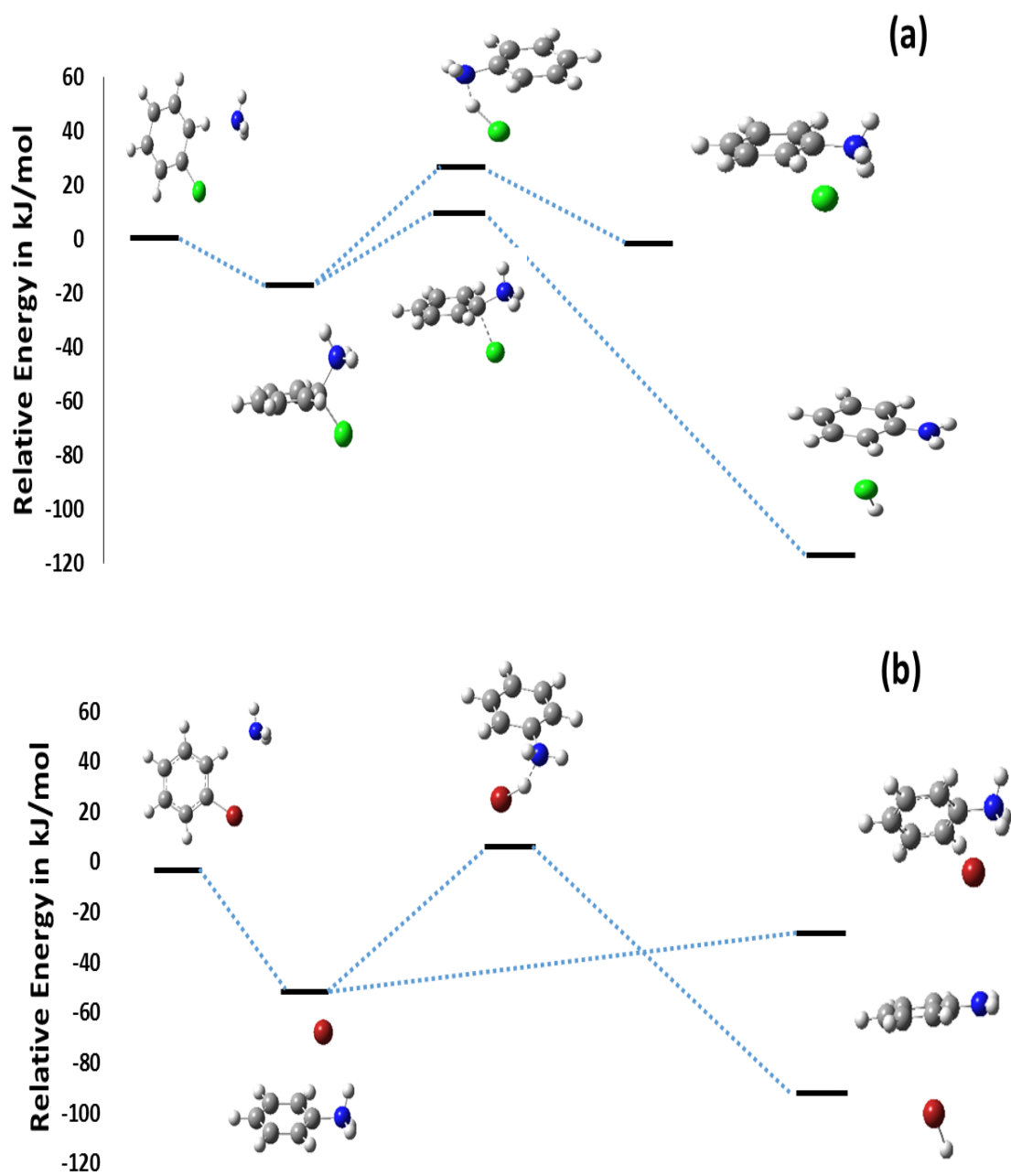


Figure 3. Upper panel: calculated stationary points on the cation radical surface of the PhCl...NH₃ system. Lower panel: similar calculations for the PhBr...NH₃ dimer.

Using the calculated stationary points on the cation radical PES, we performed microcanonical transition state theory calculations to predict the relative branching between atomic and molecular products.

The input parameters are provided in Table 1 (and A1). As the ionization energy of the $\text{PhBr}\cdots\text{NH}_3$ dimer is unknown, we estimated the dimer IP by subtracting the IP decrease observed for the $\text{PhCl}\cdots\text{NH}_3$ dimer relative to PhCl (-0.30 eV)²⁵ from the known IP of PhBr (8.98 eV).⁴⁷ Coupled with the relative calculated stationary point energies (Figure 3), we then can estimate that our two-photon energy produces the reactive intermediate with an energy of 1.25 eV ($10,100$ cm^{-1}) above its zero-point level. At this energy, the statistical branching into the molecular channel is less than 1%, much smaller than found experimentally. This again lies in contrast to the $\text{PhCl}\cdots\text{NH}_3$ system, where the experimental branching was well reproduced by statistical predictions.²⁷ What is the cause of this discrepancy? Reflecting on the distonic nature of the intermediate, we recognize that a roaming radical pathway is likely present. The roaming radical mechanism,⁴⁸⁻⁵⁰ first identified in the photodissociation of formaldehyde,⁵¹⁻⁵⁴ can occur in barrierless bond-breaking, when the departing radicals can be trapped in the relatively flat exit channel PES, and explore trajectories which lead to re-encounter and the possibility of abstraction producing molecular products.^{55,56} Essentially, a roaming path offers a different route to molecular products which bypasses the tight transition state (TS). Often a distinct rovibrational distribution is observed for the roaming products. Klippenstein *et al.* emphasize describing orientational dynamics in the long range as roaming, even when the tight TS is too high in energy to contribute, and hence no bimodal product distribution is obtained.⁵⁷

Table 1. Parameters used in microcanonical TS calculations for the Br atom loss and HBr atom loss channels.

Adduct	$E_{\text{rel}} = 0 \text{ cm}^{-1}$			
Frequencies				
3605	3603	3293	3241	3234
3229	3217	3076	1664	1663
1659	1549	1477	1429	1396
1323	1228	1168	1155	1123
1104	1075	1030	1014	999
999	847	792	693	611
551	382	360	344	286
282	257	135	133	46
42	29			
TS: Br loss	$E_{\text{rel}} = 2706 \text{ cm}^{-1}$			
Frequencies				
3489	3470	3400	3241	3234
3224	3201	3200	1695	1658
1645	1643	1538	1515	1503
1363	1338	1206	1193	1187
1122	1078	1057	1037	1024
1009	1007	938	847	793
759	653	625	525	460
406	352	300	218	200
33				
TS: HBr loss	$E_{\text{rel}} = 5352 \text{ cm}^{-1}$			
Frequencies				
3590	3496	3242	3231	3224
3214	3211	1647	1627	1586
1546	1483	1389	1374	1317
1278	1200	1187	1138	1088
1051	1048	1028	1022	1001
962	920	864	819	765
688	620	547	507	454
413	394	333	221	83
66				

In these cases the roaming fraction can be large. As the intermediate here is a distonic ion-radical complex, with no evident dissociation barrier for the radical channel, and the tight TS is much higher in energy, this is also the case here. While the majority of studies of roaming have focused on hydrogen atoms, recent studies have provided evidence for “heavy-atom (or heavy-group)” roaming.^{55,58-64} To illustrate the roaming landscape of this system, a grid of 961 (31 x 31) points were generated at the M06-2X/aug-cc-pVTZ level, describing the interaction of a Br-atom with the Ph-NH₃ cation. Figure 4 maps the interaction energy relative to separated fragments, placing the Br-atom on a square grid of points (in the plane of the heavy atoms) ranging from -7.5 to 7.5 Angstroms in both the X- and Y-directions from the center-of-mass of the Ph-NH₃ fragment. More detailed experiments such as ion imaging, are currently planned in the Marquette group, in order to gain further insight into the roaming process.

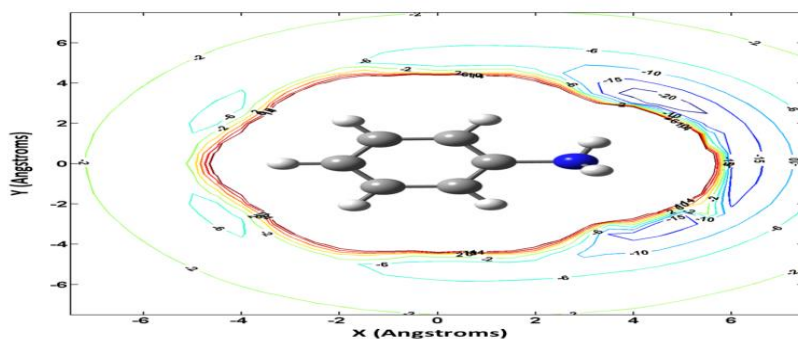


Figure 4. Contour plot of the interaction between the roaming Br-atom and the Ph-NH₃ fragment. Labeled contours indicate the energy in kJ/mol and illustrate the attractiveness of the NH₃ protons to the roaming Br-atom.

4. CONCLUSIONS

Building upon our recent studies of reactive pathways following resonant two-photon ionization in the PhCl-NH₃ dimer, we have examined the spectroscopy and dynamics of the PhBr-NH₃ dimer, for the first time. As for other PhX-NH₃ dimers, the structure of the complex found experimentally corresponds to an in-plane π -type complex, which theory confirms is the most stable minimum on the dimer PES.

Upon ionization, an intermediate is formed which reacts to yield molecular (HBr) and atomic (Br) products. As opposed to the PhCl-NH₃ system, where the cation radical intermediate formed upon ipso addition has a classic arenium ion structure, our calculations predict that the reactive intermediate in the PhBr-NH₃ system corresponds to a distonic ion-radical complex of protonated aniline and a Br atom. The calculated barrier to HBr loss is sufficiently high to render this channel insignificant (< 1%) in TST calculations, yet experiment shows a substantial (37%) branching into this channel, higher even than that observed in the PhCl-NH₃ system, where the branching was well modeled by TST. Since the tight TS is even higher in energy in this system, we rationalize these results in terms of a roaming radical mechanism for HBr formation.

REFERENCES

1. Pierangelo Metrangolo, ‡ Jane S. Murray,*,§ Tullio Pilati,† Peter Politzer,*,§ Giuseppe Resnati,†,‡ and; Terraneo†, G. *Crystal Growth & Design* **2013**.
2. Riley, K. E.; Merz, K. M., Jr. *J Phys Chem A* **2007**, *111*, 1688.
3. Politzer, P.; Murray, J. S.; Concha, M. C. *J Mol Model* **2007**, *13*, 643.

4. Tachikawa, H.; Igarashi, M. *J Phys Chem A* **1998**, *102*, 8648.
5. Barnett, R. N.; Bongiorno, A.; Cleveland, C. L.; Joy, A.; Landman, U.; Schuster, G. B. *J Am Chem Soc* **2006**, *128*, 10795.
6. Miyazaki, M.; Fujii, A.; Ebata, T.; Mikami, N. *Chem Phys Lett* **2001**, *349*, 431.
7. Harada, H.; Nagai, H.; Mine, N.; Terada, Y.; Fujiwara, H.; Mikami, I.; Tsuneizumi, M.; Yabe, A.; Miyazaki, K.; Yokota, M.; Imoto, I.; Inazawa, J.; Emi, M. *J Hum Genet* **2001**, *46*, 70.
8. Meyer, E. A.; Castellano, R. K.; Diederich, F. *Angew Chem Int Edit* **2003**, *42*, 1210.
9. Ionov, S.; Brucker, G.; Jaques, C.; Valachovic, L.; Wittig, C. *J Chem Phys* **1993**, *99*, 6553.
10. Ionov, S.; Brucker, G.; Jaques, C.; Valachovic, L.; Wittig, C. *J Chem Phys* **1992**, *97*, 9486.
11. Chen, Y.; Hoffmann, G.; Oh, D.; Wittig, C. *Chem Phys Lett* **1989**, *159*, 426.
12. Wittig, C.; Sharpe, S.; Beaudet, R. *Accounts of Chemical Research* **1988**, *21*, 341.
13. Brutschy, B. *Ber Bunsen Phys Chem* **1992**, *96*, 1154.
14. Brutschy, B.; Eggert, J.; Janes, C.; Baumgartel, H. *Journal of Physical Chemistry* **1991**, *95*, 5041.
15. Maeyama, T.; Mikami, N. *Journal of Physical Chemistry* **1991**, *95*, 7197.
16. Maeyama, T.; Mikami, N. *Journal of Physical Chemistry* **1990**, *94*, 6973.
17. Vaupel, S.; Brutschy, B.; Tarakeshwar, P.; Kim, K. S. *J Am Chem Soc* **2006**, *128*, 5416.
18. Wassermann, B.; Brutschy, B. *Journal of Molecular Structure-Theochem* **1993**, *103*, 107.
19. Riehn, C.; Lahmann, C.; Brutschy, B.; Baumgartel, H. *Ber Bunsen Phys Chem* **1992**, *96*, 1164.
20. Riehn, C.; Avdiew, J.; Eggert, J.; Wassermann, B.; Brutschy, B.; Baumgartel, H. *Journal of Molecular Structure* **1991**, *249*, 33.
21. Brutschy, B. *Journal of Physical Chemistry* **1990**, *94*, 8637.

22. Baumgartel, H.; Brutschy, B.; Ruhl, E. *Physica Scripta* **1990**, *T31*, 78.
23. Eggert, J.; Janes, C.; Wassermann, B.; Brutschy, B.; Baumgartel, H. *Ber Bunsen Phys Chem* **1990**, *94*, 1282.
24. Butterworth, K.; Chiang, C.; Cunningham, B.; Freindorf, M.; Furlani, T.; DeLeon, R.; Garvey, J. *J Phys Chem A* **2012**, *116*, 1877.
25. Grover, J.; Cheng, B.; Herron, W.; Coolbaugh, M.; Peifer, W.; JF, G. *Journal of Physical Chemistry* **1994**, *98*, 7479.
26. Tonge, N. M.; MacMahon, E. C.; Pugliesi, I.; Cockett, M. C. R. *J Chem Phys* **2007**, *126*.
27. Reid, S. A.; Nyambo, S.; Kalume, A.; Uhler, B.; Karshenas, C.; Muzangwa, L. *J Phys Chem A* **2013**, *117*, 12429.
28. Grover, J.; Herron, W.; Coolbaugh, M.; Peifer, W.; Garvey, J. *Journal of Physical Chemistry* **1991**, *95*, 6473.
29. Karlsson, D.; Borg, O.; Lunell, S.; Davidsson, J.; Karlsson, H. *J Chem Phys* **2008**, *128*.
30. Karlsson, D.; Davidsson, J. *Journal of Photochemistry and Photobiology a-Chemistry* **2008**, *195*, 242.
31. Andrejeva, A.; Tuttle, W.; Harris, J.; Wright, T. *J Chem Phys* **2015**, *143*.
32. Koplitz, B.; McVey, J. *J Chem Phys* **1984**, *80*, 2271.
33. Koplitz, B.; McVey, J. *J Chem Phys* **1984**, *81*, 4963.
34. Dietz, T.; Duncan, M.; Liverman, M.; Smalley, R. *J Chem Phys* **1980**, *73*, 4816.
35. Frisch, M. J.; Gaussian Inc.: Pittsburg, PA, 2009.
36. Zhao, Y. T., D.G *Theor. Chem. Acc.* **2008**, *120*, 215-241.
37. Mardirossian, N.; Parkhill, J. A.; Head-Gordon, M. *Phys Chem Chem Phys* **2011**, *13*, 19325.
38. Werner, H. J.; Knowles, P. J.; Knizia, G.; Manby, F. R.; Schutz, M. 2015.
39. Adler, T. B.; Knizia, G.; Werner, H. J. *J Chem Phys* **2007**, *127*.

40. Knizia, G.; Adler, T. B.; Werner, H. J. *J Chem Phys* **2009**, *130*.
41. Hill, J. G.; Peterson, K. A. *J Chem Phys* **2014**, *141*.
42. Talipov, M. R.; Boddeda, A.; Timerghazin, Q. K.; Rathore, R. *J Phys Chem C* **2014**, *118*, 21400.
43. Renz, M.; Theilacker, K.; Lambert, C.; Kaupp, M. *J Am Chem Soc* **2009**, *131*, 16292.
44. Renz, M.; Kess, M.; Diedenhofen, M.; Klamt, A.; Kaupp, M. *J Chem Theory Comput* **2012**, *8*, 4189.
45. PGOPHER **2010**.
46. Kupka, H.; Cribb, P. H. *J Chem Phys* **1986**, *85*, 1303.
47. Linstrom, P.; Mallard, W. *Journal of Chemical and Engineering Data* **2001**, *46*, 1059.
48. Bowman, J.; Suits, A. *Physics Today* **2011**, *64*, 33.
49. Bowman, J.; Shepler, B.; Sr, L.; Cremer, P.; Groves, J.; Johnson, M. *Annual Review of Physical Chemistry, Vol 62* **2011**, *62*, 531.
50. Herath, N.; Suits, A. *Journal of Physical Chemistry Letters* **2011**, *2*, 642.
51. Lahankar, S.; Chambreau, S.; Zhang, X.; Bowman, J.; Suits, A. *J Chem Phys* **2007**, *126*.
52. Suits, A.; Chambreau, S.; Lahankar, S. *International Reviews in Physical Chemistry* **2007**, *26*, 585.
53. Chambreau, S.; Townsend, D.; Lahankar, S.; Lee, S.; Suits, A. *Physica Scripta* **2006**, *73*, C89.
54. Lahankar, S.; Chambreau, S.; Townsend, D.; Suits, F.; Farnum, J.; Zhang, X.; Bowman, J.; Suits, A. *J Chem Phys* **2006**, *125*.
55. Li, H.; Tsai, P.; Hung, K.; Kasai, T.; Lin, K. *J Chem Phys* **2015**, *142*.
56. Lee, K. L. K.; Quinn, M. S.; Maccarone, A. T.; Nauta, K.; Houston, P. L.; Reid, S. A.; Jordan, M. J. T.; Kable, S. H. *Chem Sci* **2014**, *5*, 4633.
57. Klippenstein, S. J.; Georgievskii, Y.; Harding, L. B. *J Phys Chem A* **2011**, *115*, 14370.

58. Fernando, R.; Dey, A.; Broderick, B.; Fu, B.; Homayoon, Z.; Bowman, J.; Suits, A. *J Phys Chem A* **2015**, *119*, 7163.
59. Suits, A.; Fernando, R.; Dey, A. *Abstracts of Papers of the American Chemical Society* **2014**, 248.
60. Joalland, B.; Shi, Y.; Estillore, A.; Kamasah, A.; Mebel, A.; Suits, A. *J Phys Chem A* **2014**, *118*, 9281.
61. North, S.; Grubb, M.; Warter, M. *Abstracts of Papers of the American Chemical Society* **2013**, 245.
62. Joalland, B.; Van Camp, R.; Shi, Y.; Patel, N.; Suits, A. *J Phys Chem A* **2013**, *117*, 7589.
63. Grubb, M.; Warter, M.; Xiao, H.; Maeda, S.; Morokuma, K.; North, S. *Science* **2012**, *335*, 1075.
64. Xiao, H.; Maeda, S.; Morokuma, K. *Journal of Physical Chemistry Letters* **2011**, *2*, 934.

II. AN AUTOMATED THERMOCHEMISTRY PROTOCOL BASED ON EXPLICIT-CORRELATED COUPLED-CLUSTER THEORY: THE METHYL PEROXY FAMILY

Bradley K. Welch¹, Richard Dawes¹, David H. Bross^{2,3}, Branko Ruscic^{2,3}

¹Department of Chemistry, Missouri University of Science and Technology, Rolla, Missouri 65409, United States.

²Chemical Sciences and Engineering Division, Argonne National Laboratory, Argonne, Illinois 60439, United States.

³Computation Institute, University of Chicago, Chicago, Illinois 60637, United States.

ABSTRACT

An automated computational thermochemistry protocol based on explicitly-correlated coupled-cluster theory was designed to produce highly accurate enthalpies of formation and atomization energies for small to medium-sized molecular species (3-12 atoms). Each potential source of error was carefully examined and the sizes of contributions to the total atomization enthalpies were used to generate uncertainty estimates. The protocol was first used to generate total atomization enthalpies for a family of four molecular species exhibiting a variety of charges, multiplicities, and electronic ground states. The new protocol was shown to be in good agreement with the Active Thermochemical Tables database for the four species: methylperoxy radical, methoxyoxoniumylidene (methylperoxy cation), methylperoxy anion, and methyl hydroperoxide. Updating the Active Thermochemical Tables to include those results yielded significantly improved accuracy for the formation enthalpies of those species. The derived protocol was then used to predict formation enthalpies for the larger ethyl peroxy family of species.

1. INTRODUCTION

Organic peroxide thermochemistry is important to understanding atmospheric and combustion reaction networks. The simplest organic peroxy radical, methyl peroxy is an important species in the atmosphere. Methyl peroxy (CH_3O_2) reacting with nitric oxide (NO) produces about 25% of all tropospheric ozone (O_3),¹ and also leads to the production of methoxy radical (CH_3O) and nitrogen dioxide (NO_2), other components of smog.² It also reacts with hydroperoxy radical to yield CH_3OOH , and through reaction with RO_2 , is a source of atmospheric methanol. The closely related cation and anion species of the methyl peroxy are also involved in some of these reactions, and therefore accurate enthalpies are desirable for the entire family of compounds.¹ A recent study showed that methyl peroxy is behind the most plausible explanation for the formation of the simplest Criegee intermediate (carbonyl oxide).³ To enable high accuracy studies of these species a comprehensive description of the thermochemistry of methyl peroxy, related species, and larger peroxy species is necessary.

Composite thermochemistry calculations have been developed that offer accuracy far beyond what can be affordably achieved in any single calculation. Recent high accuracy composite methods such as the various HEAT protocols,^{4,5} the W4 family,⁶ as well as the FPD⁷ approach offer the ability to obtain 2σ uncertainties⁸ in computed 0 K enthalpies of formation less than 1 kJ mol^{-1} in favorable cases, far exceeding the common “chemical accuracy” target of 1 kcal/mol (4.18 kJ mol^{-1}). These approaches rely on composite schemes to compute various components of the total energy separately. In general, different computational methods are applied to each contribution which permits tuning of the overall cost and accuracy. Reliable data is necessary for accurate kinetics

computations involving many intermediates. Relatively small errors can significantly impact computed reaction barriers and associated rates. Explicit consideration of numerous reaction steps is common in accurate models of atmospheric processes, combustion, as well as interstellar chemistry. While these composite protocols can obtain highly accurate thermochemical values, they are still challenging to use for larger species primarily due to their poor scaling with respect to the number of electrons and nuclei. The original HEAT protocol as well as the W4 method are currently limited to small systems of only a few heavy atoms. Recent developments such as the perturbative quadruples method [CCSDT(Q)]⁹ as well as general improvements to computer hardware have allowed these protocols to be extended. An application of the HEAT approach to a medium sized molecule was reported by Harding *et al.* in a study of benzene.¹⁰ Another direction in protocol development for larger systems involves developing scaling procedures and extrapolations to permit use of smaller bases for the most expensive terms. This is seen in methods such as the W3X, W3X-L, ANO-0, ANO-F12 and diet-HEAT-f12 methods.¹¹⁻¹⁴ These approximations help control costs for larger molecules. There are several reported thermochemical protocols that employ explicitly-correlated coupled-cluster (F12) theory in some way (W1-F12,¹⁵ W3-F12,¹⁶ W4-F12,¹⁶ and diet-HEAT-F12⁶ as examples).

Owing to the central role of thermodynamics, there is a long history of efforts to compile the currently available thermodynamic data into tabulations usable by the broader scientific community. The nature of these lists is reviewed in detail elsewhere,¹⁷ but even the best critically evaluated compilation has the severe limitation that it cannot be easily updated with new information because of the nature of their sequential

construction. Traditional thermochemical determinations are also usually based upon a single set of experiments or computational result. In a departure from this, the Active Thermochemical Tables approach (ATcT) of Ruscic *et al.*^{18,19} enables seamless updates and uses all of the available information to yield a self-consistent set of thermochemical values. The ATcT approach relies on construction of the thermochemical network (TN) from all determinations and self-consistently solves the TN leading to more accurate set of thermodynamic values.¹⁸⁻²⁰ ATcT has driven down the uncertainty for most species contained within it to at least an order of magnitude better than previous efforts, with small molecules having uncertainties frequently less than 1 kJ mol⁻¹ and in some cases below 0.1 kJ mol⁻¹.²⁰ Through this reduction in uncertainty, ATcT has in turn provided the critical benchmarks that are necessary prerequisites for developing new high accuracy composite methods. To streamline the generation of accurate thermochemical data for these and other species, and to facilitate their introduction to the ATcT network, we have developed an automated computational workflow. Based on explicitly-correlated coupled-cluster theory, and governed by Python scripts, a protocol was developed and benchmarked through application to the methyl peroxy family of species, validated through consistency with the existing ATcT database as well as other experimental and computational results.

2. COMPUTATIONAL DETAILS

A complete composite method necessarily includes all contributions that are significant within the desired accuracy for the species of interest. Since the desired accuracy target here is to exceed chemical accuracy (1 kcal/mol), this requires

sufficiently accounting for valence electron correlation, core electron correlation, zero-point vibrational energy (ZPVE), higher-order electron correlation (HOC), relativistic effects, and non-adiabatic effects through a Diagonal Born-Oppenheimer Correction (DBOC). These various terms are illustrated in Figure 1, which is a flowchart of the new procedure.

Throughout this work conventional and explicitly-correlated (F12) coupled cluster calculations were carried out. For the explicitly-correlated valence electron calculations the cc-pVnZ-F12 ($n=T, Q, 5$) basis sets were used while the core-valence calculations were carried out with the cc-pCVnZ-F12($n=T, Q$) family of basis sets.²¹⁻²³ For each basis, the default recommended auxiliary CABS, and RI basis sets developed for use with each of these sets were used respectively, along with the same geminal slater exponent of 1.4 for the valence calculations and for the core-valence calculations.¹⁹⁻²¹ The explicitly-correlated calculations used the F12b method of Werner and coworkers²⁴ along with the fixed amplitude 3C(FIX)25 ansatz. The conventional coupled-cluster calculations were carried out using cc-pVnZ ($n=D, T$), aug-cc-pVTZ, and aug-cc-pCVTZ²⁶ basis sets. All CCSD(T)-F12b computations were performed with MOLPRO 2015²⁷ using tighter than default gradient and energy convergence criteria of 10^{-5} and 10^{-10} respectively. For open-shell species the ROHF/UCCSD(T)-F12b variant was used. For open-shell species the ROHF reference was used for the HOC term for consistency with the other calculations. HOC calculations beyond CCSD(T) were carried out using CCSDT and CCSDT(Q) with MRCC.^{28,29} For open-shelled species, the *B* ansatz is specified for (Q).³⁰ VPT2 calculations were performed with the SURF code in MOLPRO.^{31,32}

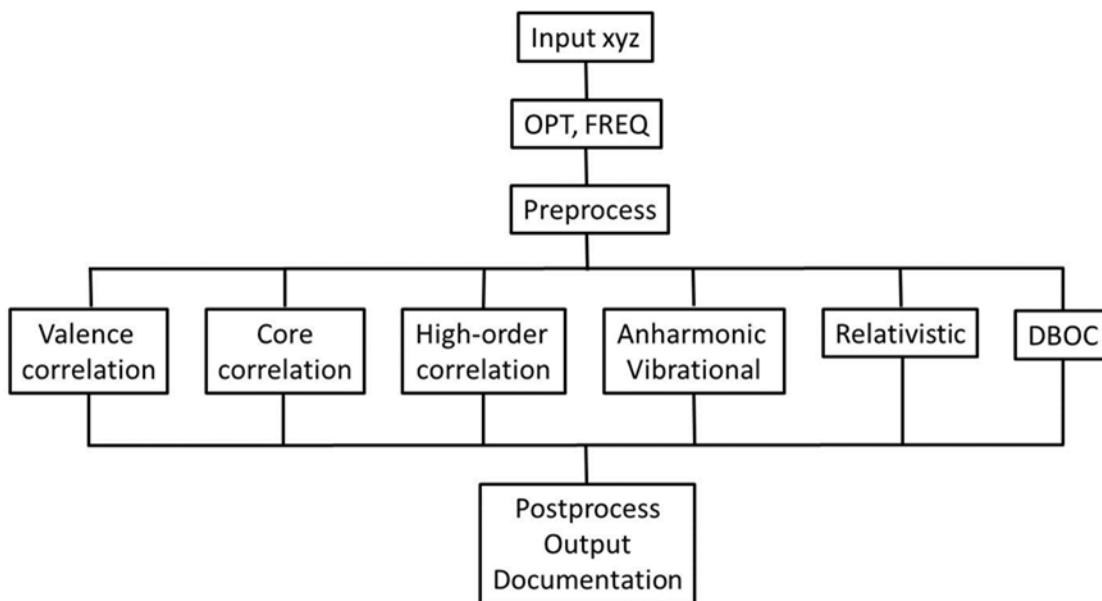


Figure 1. Flowchart of the automated thermochemical protocol. Details of each contribution to the composite energy and the pre- and post-processing procedures are given in the text.

Our newly developed composite thermochemistry approach is the following: 1) the molecular geometry is optimized with CCSD(T)-F12b/cc-pVTZ-F12, 2) the anharmonic ZPVE as well as fundamental vibrational levels are computed using VPT233 with resonances analyzed and removed at the CCSD(T)-F12b/cc-pVTZ-F12 level, 3) CCSD(T)-F12b/cc-pVnZ-F12 ($n=T-5$) are carried out to obtain the HF and valence correlation energies, 4) the core correlation contribution is defined as the energy difference between all electron and valence only CCSD(T)-F12b/cc-pCVnZ-F12($n=T, Q$) calculations, 5) the HOC contribution is calculated as the sum of ΔT and ΔQ with $\Delta T = \text{CCSDT} - \text{CCSD(T)}$ using the cc-pVTZ basis set and $\Delta Q = \text{CCSDT(Q)} - \text{CCSDT}$ using the cc-pVDZ basis set, 6) the contribution of scalar relativistic effects is calculated as the expectation values of the mass-velocity and one-electron Darwin operators using

CFOUR³⁴ at the CCSD(T)/aug-cc-pCVTZ level of theory, 6) DBOC is calculated using ROHF with the aug-cc-pVTZ basis set with CFOUR³⁵ 7) Spin-orbit contributions are included for atomic spin-orbit coupling.⁴ None of the molecular species considered here have first-order SO effects, so SO effects were not considered further.

The above protocol has been automated and gives the total energy as:

$$E = E_{HF} + E_{CCSD} + E_{(T)} + E_{Core} + E_{HOC} + E_{Rel} + E_{ZPVE} + E_{DBOC} + E_{SO} \quad (1).$$

The automated protocol, governed by Python scripts is flexible in its implementation and so results for a variety of different procedures are compared. For *procedure 1*, the core-correlation term and the HOC term both include only the largest employed single basis (without extrapolation), whereas for *procedure 2*, each of those contributions is extrapolated. *Procedure 3* and *Procedure 4* are similar to *Procedures one* and *two* with a key exception. The structure and harmonic frequencies are obtained with CCSD(T)-F12b and the PVDZ-F12 basis set. This combination has been shown to give good harmonic ZPVE's.³⁶ Rather than use CCSD(T)-VPT2, the VPT2 correction is obtained with B3LYP and the cc-pvtz basis set of Dunning. The VPT2 procedure in Gaussian 0937 is described by Barone.³⁸ The automated procedure starts with an inputted approximate Cartesian structure and begins by performing an optimization and harmonic frequency calculation. In what is labeled *preprocess* in the flowchart of Figure 1, the optimized geometry is recorded, and the harmonic frequencies are checked for imaginary or low-frequency modes (floppy modes might introduce significant error into the anharmonic vibrational contribution). The T_1 diagnostic is also recorded as a possible indication of multireference character. Next, the optimized geometry is passed forward,

and the six contributions to the total energy are computed separately using various different codes and resources, with allocations balanced by consideration of the relative cost, efficiency of parallelization etc. Once completed, the timing for each contribution is recorded, and to help confirm proper convergence, the value recorded for each term is assessed to ensure that it is within a reasonable range. A few additional tests are made including looking at the percentage contribution of HOC to the total atomization energy, as well as looking for unusually large anharmonic corrections to the vibrational frequencies. These steps correspond to the *post-processing* of Figure 1. All of this is done automatically using Python scripting and in addition to producing a master output summarizing the results (including the derived enthalpy of formation and atomization energy).

CBS extrapolations were carried out using three different formulas including the l^3 approach ($E_n^{corr} = E_{CBS}^{corr} + \frac{A}{l_{max}^3}$), employing the two largest basis set used in a given term. The uncertainty of extrapolation is estimated using the statistics of three different schemes: the l^3 approach,³⁹ a Schwenke extrapolation procedure,⁴⁰ and an l^4 extrapolation method.⁴¹ The coefficients for the extrapolation using Schwenke's formula are those derived by Hill *et al.*⁴² The Schwenke extrapolated (T) term was used in the composite energy. Our approach separated the CCSD and (T) terms primarily to account for differences in the convergence behavior of CCSD vs (T) energies due to explicit correlation of CCSD. A similar approach has been used by Feller to determine uncertainties in other highly accurate computed enthalpies of formation.^{43,44}

Enthalpies of formation for 0 K and 298 K were determined by first computing the atomization energy of the molecule in question, and then determining the enthalpy of

formation via the difference between the reference atomic enthalpies of formation and the atomization energy (the same approach was used in reference 7). The enthalpies of formation for the atomic species was taken from reference 25, the current Active Thermochemical Tables.

3. RESULTS AND DISCUSSION

The HF term has previously been shown to be well converged towards the CBS limit with the large basis set (cc-pV5Z-F12) employed in this work.²¹ We also found that non-extrapolated CCSD-F12b with the cc-pV5Z-F12 basis paired with an extrapolation of the (T) term using the VTZ-F12 and VQZ-F12 basis sets and a Schwenke extrapolation,^{37,39} yields well-converged results compared with higher cost benchmarks. For most of the other terms in the composite scheme, uncertainty contributions were determined as half the difference to the next larger possible basis computation. For the DBOC term, no uncertainty was assigned this way due to DBOC's weak basis set dependence,⁴⁰ and while CCSD/DBOC is feasible with CFOUR, our tests found the contribution beyond ROHF in the correlation hierarchy to be negligible.

Table B1 summarizes the energy contributions for each species considered in this study. A version of ATcT TN denoted 1.122-q-pre was initially constructed from the previously existing thermochemical data mentioned in the introduction, and these, along with the results of several standard mid-level computations (such as CBS-APNO, G3X, G4, CBS-QB3), were used to benchmark the composite protocol developed here. The thermochemical data for reactions involving methyl peroxy included in this version of the TN are detailed in Table 2.²⁰ After inclusion of the new results, the resulting

recommended enthalpies of formation from a version of ATcT TN denoted 1.122q, based on these reactions and the current work is given in Table 6. Table 7 compares the anharmonic vibrational frequencies computed with VPT2 with experimental assignments where available. Although experimental data is somewhat limited for these species (altogether only 13 fundamental frequencies), the level of agreement is impressive, instilling confidence in what can easily be a rather large source of overall error. Not only is the root-mean-squared deviation (RMSD) low (5.61 and 2.51 cm^{-1} for CH_3O_2 radical and $\text{CH}_3\text{O}_2\text{H}$ respectively), but the errors are distributed about the mean leading to some cancelation of error in the overall ZPVE contribution.

3.1 METHYLPEROXY RADICAL

The methylperoxy radical (doublet) has received significant attention in the literature due to its importance in atmospheric and combustion processes.^{2,45-52} Table 2 summarizes available reaction thermochemistry for it. A variance decomposition approach, which reveals the detailed provenance of the ATcT results,^{40,53} shows that the primary contributor to the enthalpy of formation of methyl peroxy in TN version 1.122q-pre is the HEAT345(Q) determination of Nguyen *et al.* for the dissociation of methyl peroxy into methyl and oxygen,⁵⁴ and an enthalpy of CH_3 which has already been well established.⁵⁹ This determination accounts for 41% of the variance, and is consistent with a third-law analysis performed on the experimental data of Slagle and Gutman.⁵⁵ A third-law analysis of Knayzev and Slagle⁵⁶ yields a reaction enthalpy that is 2.3 kJ/mol above that reported by Slagle and Gutman and 4.3 kJ/mol above the HEAT345(Q) value, but

indeed an ATcT analysis finds the reported 2.1 kJ/mol error bar likely underestimates the uncertainty by a factor of 1.8.

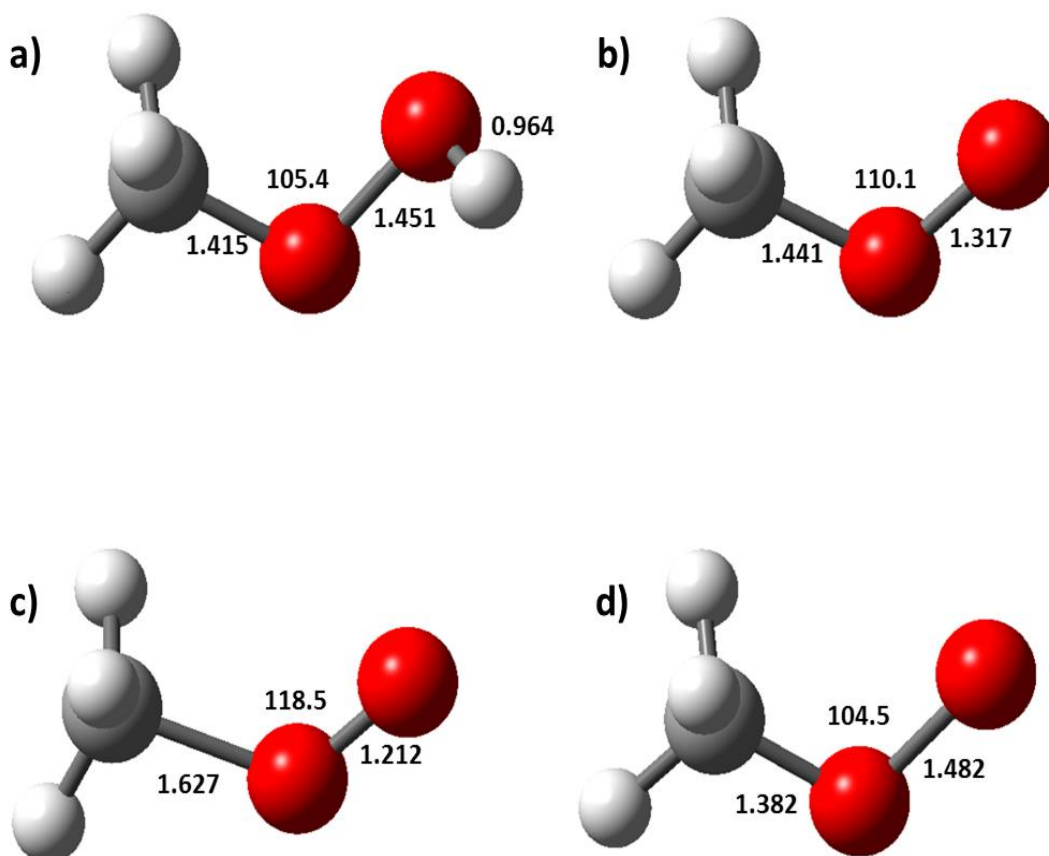


Figure 2. Some relevant structural parameters for members of the methyl peroxy family (distances in Angstroms and angles in degrees). CH_3O_2 structures b), c) and d) are those of the neutral radical, cation, and anion systems respectively.

Second-law analyses by Slage and Gutman and Knayzey and Slage yield values that are consistent with all three values, given uncertainties that are so large that these reactions do not appreciably contribute to provenance. There is also a determination of the equilibrium constant of methylperoxy and methyl from Khachatryan *et al.* that is also consistent with these determinations.⁵⁷ There are two photoionization appearance energies of methylium from methyl peroxy that are also consistent with this enthalpy of formation.⁴⁶⁻⁴⁷ There are other theoretical determinations included in the network that are also consistent, but the distributed provenance of methyl peroxy across several consistent experimental determinations, in addition to the well-established enthalpy of formation of methyl and methylium gives confidence that the heat of formation of methyl peroxy is well established in TN version 1.122q-pre. Our current computational results agree well with the HEAT-345(Q) results of Nguyen *et al.*,⁵¹ the ANL0 results of Klippenstein *et al.*,¹³ the CCSD(T) results of Shallcross *et al.*,⁴⁵ and the results of ATcT TN version 1.122q-pre. The results of the present calculations were added to the TN, resulting in ATcT TN version 1.122q, which unsurprisingly yielded a similar enthalpy of formation for methyl peroxy to the prior version, albeit with a slightly smaller uncertainty owing to the additional high accuracy composite thermochemistry results added from this work.

3.2. METHOXYOXONIUMYLIDENE (METHYL PEROXY CATION)

The structure of the (triplet) cation species is shown in Figure 2. Interestingly, the C-O bond is very long at 1.63 Å, while the O-O bond length is quite short (close to that of a free O₂ diatomic). Methoxyoxoniumylidene is the photoionization product of the methylperoxy radical,⁴⁶⁻⁴⁷ and has been observed by mass spectrometry.⁵⁸ Interestingly

the methylperoxy cation is the only known stable alkyl peroxy cation (the larger ones have not been found to be stable).⁵⁶ The photoionization⁴⁷ and photoelectron⁴⁶ observations of methoxyoxoniumylidene from methyl peroxy, in combination with mid-level composite theory results (W1RO, CBS-APNO, G3X, G4, CBS-QB3) and the provenance of methyl peroxy mentioned above yielded the majority of the provenance of CH_3OO^+ . The resulting reaction enthalpies shown in table 2 are in excellent agreement with the present results.

3.3. METHYL HYDROPEROXIDE

Methyl hydroperoxide has received a large amount of attention both experimentally and computationally due to its role in NO_2 production in the atmosphere.⁵⁹⁻⁶⁵ The optimized structure obtained in this work is shown in Figure 2. The geometry of the heavy-atom backbone is similar to that of the CH_3O_2 anion discussed next. Matthews *et al.* determined the onset of methoxy and hydroxyl from methyl hydroperoxide via laser induced fluorescence and reported two values, one from the maximum OH excitation energy, and the other from the average.⁶² These determinations are consistent with, but less accurate than the theoretical determination of the enthalpy in the same work, which is the dominant contributor to the provenance of the enthalpy of formation of CH_3OOH at 9%. Generally the provenance of CH_3OOH is well distributed including the above reactions, a photoelectron study,⁶⁶ and a variety of theoretical determinations.^{13,67} the gas phase acidity of Blanksby *et al.*⁶⁸ is inconsistent with the remainder of the thermochemical network, and our statistical analysis increases their reported error bar by a factor of three. Our present computational results agree well with

the CHEAT results of Faragó *et al.*,⁶⁴ the ANL0 results of Klippenstein *et al.*,¹³ and the results of ATcT TN version 1.122q-pre.

3.4. METHYLPEROXY ANION

Table 1 and 2 summarizes the results for this singlet species. The structure is shown in Figure 2 and is most similar to that of the back-bone of methyl hydroperoxide. Compared to the other members of the family studied in this work, this species has received comparably little attention. The initial network TN version 1.122q-pre was constructed with the reactions shown in Table 2. The photoelectron results from Blanksby *et al.*⁶⁵ are consistent with mid-level composite theory results (CBS-APNO, G3X, G4, CBS-QB3), and due to the small uncertainty of those results this determination alone accounts for 43% of the provenance of methylperoxy anion. The remaining provenance is primarily distributed over reactions that were described in the determination of the enthalpy of formation of methyl peroxide. Our current computational results agree well with Blanksby *et al.* and ATcT 1.122q-pre.

3.5. ETHYLPEROXY RADICAL

Figure 3 shows the structure of the Ethyl Peroxy radical as well as the other ethyl species. Table 3 summarizes our results. The Ethylperoxy radical like the smaller RO₂ can isomerize to QOOH species under auto-ignition conditions.⁶⁹⁻⁷¹ These QOOH can then decompose to other species. Due to its importance in combustion like its smaller relative (CH₃O₂), having an accurate thermochemical value is of importance to modeling combustion kinetics. The species has also been studied via ring down cavity spectroscopy

to understand its spectra.⁷² The Photodynamics have been studied to understand how it fragments in different channels.

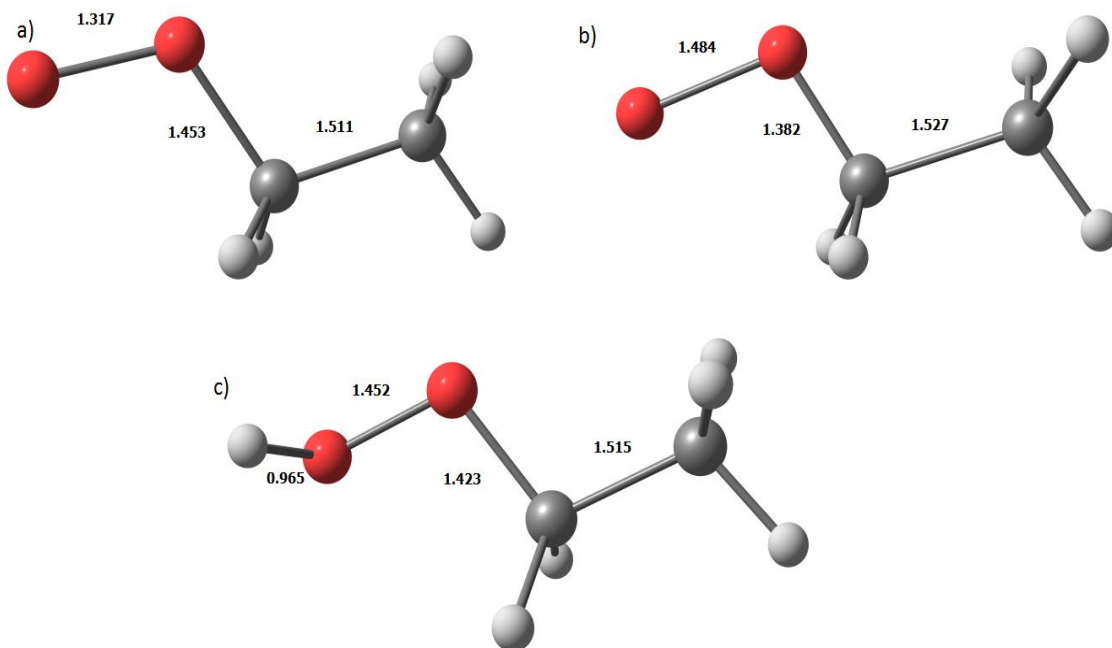


Figure 3. Some relevant structural parameters of the Ethyl Peroxy and Hydroperoxide species. a.) being the radical, b.) the anion, and c.) the hydroperoxide species.

Unlike its methylperoxy sibling, ethylperoxy has a notable three body dissociation channel.⁶⁹ Our ΔH_o 's for *procedures 3* and *4* compare well with the work of Klippenstein *et al.*¹³ Their values are slightly more negative than ours, though still consistent (-5.56 ± 2.19 and -4.73 ± 1.38 kJ mol^{-1} vs. -6.1 and -5.9 kJ mol^{-1} for ANO0 and ANO0-F12). Similarly they are high level computations that include HOC, DBOC, and explicit anharmonic corrections rather than scaling harmonic zero point energies. The reduced uncertainty for *procedure 4* is from extrapolating the T and CV terms rather than stopping with a particular basis set. The error would then come from comparing a

CCSDT/PVTZ computation to a CCSDT/(DZ,TZ) CBS extrapolation vs. CCSDT/DZ vs CCSDT/PVTZ. The latter leads to a greater difference. This trend is seen with the methyl family with all four procedures. Our work also agrees well with the 0 K obtained from ref 52's approach (-5.00 ± 3.77 kJ mol⁻¹) though our approach has a smaller uncertainty. Comparatively there is more 298 K data available. Ref 69's enthalpy is extracted from a kinetics study by Knyazev and Slagle. The enthalpy they obtained was $\Delta_f H_{298} = -27.19 \pm 10.14$ kJ mol⁻¹ which our $\Delta_f H_{298}$ of -27.27 ± 2.19 and -26.45 ± 1.38 kJ mol⁻¹ are in good agreement with. In terms of computational work our work is in disagreement with ref 52 (-20.92 ± 3.77 kJ mol⁻¹ vs -27.27 ± 2.19 and -26.45 ± 1.38 kJ mol⁻¹) while ref's 63 and 68 are more in line with our values. This is interesting due to the fact that the work in ref 44 uses a Bond Additivity Correction (BAC) trained via the ATcT. Our 0 K enthalpy was also consistent with their 0 K enthalpy. None-the-less, all of these values obtained computationally are necessary for constructing an enthalpy of formation for a new addition to the ATcT. All of these results are summarized in Table 6.

It should be noted that a trend became evident with the methylperoxy results for all 4 procedures. Procedures 1 and 3 were in better agreement with the ATcT compared to 2 and 4. At first this seemed strange, but the change was due to procedure 2 involving the CCSDT CBS extrapolation. What we suspect is it's due to some compensation between the CCSDT/PVTZ and (Q)/PVDZ terms. None-the-less both procedures need to be evaluated within the context of the ATcT network and whether one or the other is an outlier or has less of a provenance for ethylperoxy.

3.6. ETHYL HYDROPEROXIDE

Table 4 summarizes our results for this species. Ethyl hydroperoxide is produced when ethylperoxy abstracts hydrogen from stable molecules. Ethyl hydroperoxide decomposes under combustion conditions via the reaction of $\text{CH}_3\text{CH}_2\text{OOH} \rightleftharpoons \text{CH}_3\text{CH}_2\text{O} + \text{OH}$.⁷³ It can also react with radicals. The alkyl hydroperoxides have been suggested to be a source of chain-branching in the low temperature combustion regime.⁷⁴ It also has been shown to be an importance source of the hydroxyl radical in the atmosphere.⁵⁶

Our results are summarized in Table 7 along with literature results. For 0 K enthalpies our values are -142.23 ± 2.30 and -141.25 ± 1.39 kJ mol⁻¹. This is in good agreement with the values of Klippenstein *et al.*¹³ which are composite post CCSD(T) approaches. Our approach is also in good agreement with the cheaper approach of Ref 52. Going to the 298 K results, our values are technically in agreement with the bomb calorimetry of Stathis and Egerton due to the large uncertainty.⁷⁵ Knowing that hydroperoxide species are notoriously unstable and considering these computational results the experiment should be reevaluated. In terms of computational results for 298 K our procedures agree well with ref 68. Our values are in agreement with Ref 52 with the note that our error bars barely overlap. Our values are in better agreement with the average of four lower level approaches of Bozzelli and Wang.⁶³ A challenge with this system is the fact that it has both a CCOO torsion and a COOH torsion. This warrants future study, especially if partition function quantities are to be derived due to being sensitive to inaccurate treatments of low energy modes.

3.7. ETHYLPEROXY ANION

Table 5 summarizes our results. The ethylperoxy anion has received minimal attention compared to the other species. This is due to the lack of stability. None-the-less the negative-ion photoelectron spectra has been recorded and the electron attachment obtained. Blanksy et.al obtained an EA of 1.186 ± 0.004 eV.⁶⁸ This converts to a $\Delta H_{\text{rxn},0} = 114.432 \pm 0.386$ kJ mol⁻¹. Using our procedure 3 and 4 enthalpies of formation we obtain for procedure 3 of $\Delta H_{\text{rxn},0} = 112.90 \pm 3.45$ and for procedure 4 $\Delta H_{\text{rxn},0} = 112.63 \pm 2.18$. Both procedures are in good agreement with the electron attachment energy. For the $\Delta H_{\text{f},298\text{K}}$ we obtain from Blanksby *et al.*⁶⁸ -142.88 ± 9.62 kJ mol⁻¹ which is in agreement with our values for procedure 3 and 4. These results are summarized in table 8.

4. CONCLUSION

We present a flexible automated thermochemical computational protocol based on explicitly-correlated coupled-cluster theory designed to generate benchmark level enthalpies of formation and atomization energies for small to medium-sized molecular species. The workflow is governed by Python scripts and includes flexible components of a newly derived composite energy scheme including valence, core, and high-order electron correlation, as well as anharmonic vibrational levels, and corrections for relativistic and non-Born-Oppenheimer effects. All of the codes are run automatically, as well as post-processing of results, including convergence checks and documentation of all input and output files.

The procedure was demonstrated on the smallest family of alkyl peroxide and hydroperoxide species, the methyl family. Enthalpies of formation were calculated at 0 K

and 298 K and compared with other calculations, experiments and the existing ATcT network. The new values are consistent with the current ATcT database. Conservative uncertainties are assigned to the calculated data as part of the procedure and these were found to overlap with those of the existing network. The agreement between the data for the methyl peroxy species gives confidence to the predictions made for ethyl peroxy species.

This new validated automated procedure is a convenient way for the ATcT network to expand in a community driven way as the workflow can be applied to a variety of species of interest, and the results so obtained can be interfaced to update the network.

ACKNOWLEDGEMENT

The work at Argonne National Laboratory was supported by the U.S. Department of Energy, Office of Science, Office of Basic Energy Sciences, Division of Chemical Sciences, Geosciences and Biosciences, under Contract No. DE-AC02-06CH11357, through the Gas-Phase Chemical Physics Program (BR) and the Computational Chemical Sciences Program (DHB). This research used resources of the Argonne Leadership Computing Facility, which is a DOE Office of Science User Facility supported under Contract DE-AC02-06CH11357.

We gratefully acknowledge computing resources provided by Bebop, a high-performance computing cluster operated by the Laboratory Computing Resource Center

at Argonne National Laboratory. B.W. and R.D. are supported by the U.S. Department of Energy, Office of Science, Office of Basic Energy Sciences, Grant no. DE-SC0019740.

REFERENCES

1. Müller, J.-F. C. A.; Liu, Z.; Nguyen, V. S.; Stavrakou, T.; Harvey, J. N.; Peeters, J. The reaction of methyl peroxy and hydroxyl radicals as a major source of atmospheric methanol. *Nature Communications* **2016**, *7*, 13213.
2. Launder, A. M.; Agarwal, J.; Schaefer, H. F. Exploring Mechanisms of a Tropospheric Archetype: $\text{CH}_3\text{O}_2 + \text{NO}$. *J. Chem. Phys.* **2015**, *143*
3. Nguyen, L.T; McCarthy, C.M; Stanton, F.J.; Relatively Selective Production of the Simplest Criegee Intermediate in a CH_4/O_2 Electric Discharge: Kinetic Analysis of a Plausible Mechanism. *J. Phys. Chem. A* **2015**, *28*, 7197-7204.
4. Tajti, A.; Szalay, P. G.; Császár, A. G.; Kállay, M.; Gauss, J.; Valeev, E. F.; Flowers, B. A.; Vázquez, J.; Stanton, J. F. HEAT: High accuracy extrapolated ab initio thermochemistry. *J. Chem. Phys.* **2004**, *121*, 11599–11613.
5. Harding, M. E.; Vázquez, J.; Ruscic, B.; Wilson, A. K.; Gauss, J.; Stanton, J. F. High-Accuracy extrapolated ab initio thermochemistry. III. Additional improvements and overview. *J. Chem. Phys.* **2008**, *128* (11), 114111–114111-15.
6. Karton, A.; Rabinovich, E.; Martin, J. M. L.; Ruscic, B. W4 theory for computational thermochemistry: In pursuit of confident sub-KJ/Mol predictions. *J. Chem. Phys.* **2006**, *125* (14), 144108.
7. Peterson, K. A.; Feller, D.; Dixon, D. A. Chemical accuracy in ab initio thermochemistry and spectroscopy: Current strategies and future challenges. *Theor. Chem. Acc.* **2012**, *131*, 1079–1099.
8. Ruscic, B.; Uncertainty quantification in thermochemistry, benchmarking electronic structure computations, and Active Thermochemical Tables. *Int. J. Quantum Chem.* **2014**, *114*, 1097–1101.

9. Kállay, M. C. A.; Gauss, J. Approximate treatment of higher excitations in coupled-Cluster theory. II. Extension to general single-Determinant reference functions and improved approaches for the canonical Hartree–Fock case. *J. Chem. Phys.* **2008**, *129*(14), 144101.
10. Harding, M. E.; Vázquez, J.; Gauss, J.; Stanton, J. F.; Kállay, M. Towards highly accurate ab initio thermochemistry of larger systems: Benzene. *J. Chem. Phys.* **2011**, *135* (4), 044513.
11. Ganyecz, C. C. A.; Kállay, M.; Csontos, J. Moderate-Cost Ab Initio Thermochemistry with Chemical Accuracy. *J. Chem. Theory Comput.* **2017**, *13*, 4193–4204
12. Chan, B.; Radom, L. *J. Chem. Theory Comput* **2013**, *9*, 4769– 4778.
13. Klippenstein, S. J.; Harding, L. B.; Ruscic, B. Ab Initio Computations and Active Thermochemical Tables Hand in Hand: Heats of Formation of Core Combustion Species. *J. Phys. Chem. A* **2017**, *121*, 6580–6602.
14. Chan, B.; Radom, L. W2X and W3X-L: Cost-Effective Approximations to W2 and W4 with kJ mol⁻¹ Accuracy. *J. Chem. Theory Comput* **2015**, *11*, 2109–2119.
15. Karton, A.; Martin, J. M. L. Explicitly correlated W_n theory: W1-F12 and W2-F12. *J. Chem. Phys.* **2012**, *136*, 124114.
16. Sylvetsky, N.; Peterson, K. A.; Karton, A.; Martin, J. M. L. Toward a W4-F12 approach: Can explicitly correlated and orbital-Based ab initio CCSD(T) limits be reconciled? *J. Chem. Phys* **2016**, *144*, 214101.
17. Chase, M. W., Jr.; Davies, C. A.; Downey, J. R., Jr.; Frirup, D. J.; McDonald, R. A.; Syverud, A. N. *NIST-JANAF Thermochemical Tables, 4th edition*, *J. Phys. Chem. Ref. Data Monogr.* **1998**, *9*.
18. Ruscic, B.; Pinzon, R. E.; Morton, M. L.; Laszewski, G. V.; Bittner, S. J.; Nijssure, S. G.; Amin, K. A.; Minkoff, M.; Wagner, A. F. Introduction to Active Thermochemical Tables: Several “Key” Enthalpies of Formation Revisited†. *J. Phys. Chem. A* **2004**, *108*, 9979–9997.
19. Ruscic, B.; Pinzon, R. E.; von Laszewski, G.; Kodeboyina, D.; Burcat, A.; Leahy, D.; Montoya, D.; Wagner, A. F. Active Thermochemical Tables: Thermochemistry for the 21st Century. *J. Phys. Conf. Ser.* **2005**, *16*, 561–570.

20. Ruscic, B.; Bross, D. H. *Active Thermochemical Tables (ATcT) values based on ver. 1.122 of the Thermochemical Network* **2016**; available at ATcT.anl.gov
21. Peterson, K. A.; Adler, T. B.; Werner, H.-J. Systematically convergent basis sets for explicitly correlated wavefunctions: The atoms H, He, B–Ne, and Al–Ar. *J. Chem. Phys.* **2008**, *128*, 084102.
22. Hill, J. G.; Mazumder, S.; Peterson, K. A. Correlation consistent basis sets for molecular core-Valence effects with explicitly correlated wave functions: The atoms B–Ne and Al–Ar. *J. Chem. Phys.* **2010**, *132*, 054108.
23. Peterson, K. A.; Kesharwani, M. K.; Martin, J. M. The cc-pV5Z-F12 basis set: reaching the basis set limit in explicitly correlated calculations. *Molecular Physics* **2014**, *113*, 1551–1558.
24. Adler, T. B.; Knizia, G.; Werner, H.-J. A Simple and efficient CCSD(T)-F12 approximation. *J. Chem. Phys.* **2007**, *127*, 221106-3
25. Werner, H.-J.; Adler, T. B.; Manby, F. R., *J. Chem. Phys.* **2007**, *126*, 164102-18
26. Woon, D. E., Dunning T. H. Jr.; Gaussian Basis sets for use in correlated molecular calculations. V. Core-valence basis sets for boron through neon. *J. Chem. Phys.* **1995**, *103*, 4572-4585.
27. Werner, H.-J.; Knowles, P. J.; Knizia, G.; Manby, F. R.; Schutz, M.; Celani, P.; Korona, T.; Lindh, R.; Mitrushenkov, A.; Rauhut, G.; et al. *MOLPRO*, version 2015.1, A Package of Ab Initio Programs; see <http://www.molpro.net>.
28. Kállay, M.; Gauss, J. Approximate Treatment of Higher Excitations in Coupled-Cluster Theory. *J. Chem. Phys.* **2005**, *123*, 214105.
29. Kállay, M. MRCC, A String-Based Quantum Chemical Program Suite
30. Kállay, M. C. A.; Gauss, J. Approximate treatment of higher excitations in coupled-Cluster theory. II. Extension to general single-Determinant reference functions and improved approaches for the canonical Hartree–Fock case. *J. Chem. Phys.* **2008**, *129*(14), 144101.
31. Rauhut, G. Efficient Calculation of Potential Energy Surfaces for the Generation of Vibrational Wave Functions. *J. Chem. Phys.* **2004**, *121*, 9313.

32. Hrenar, T.; Werner, J. H.; Rauhut, G. Accurate Calculation of Anharmonic Vibrational Frequencies of Medium Sized Molecules Using Local Coupled Cluster Methods. *J. Chem. Phys.* **2007**, *126*, 134108.
33. Ramakrishnan, R.; Rauhut, G. Semi-Quartic Force Fields Retrieved from Multi-Mode Expansions: Accuracy, Scaling Behavior, and Approximations. *J. Chem. Phys.* **2015**, *142*, 154118.
34. Stanton, J. F.; Gauss, J.; Harding, M. E.; Szalay, P. G., with contributions from Auer, A. A.; Bartlett, R. J.; Benedikt, U.; Berger, C.; Bernholdt, D. E.; Bomble, Y. J.; et al., and the integral packages *MOLECULE* (Almlöf, J.; Taylor, P. R.), *PROPS* (Taylor, P. R.), *ABACUS* (Helgaker, T.; Jensen, H. J.; Jørgensen, P.; Olsen, J.), and ECP routines by Mitin, A. V.; van Wüllen, C. For the current version, see: <http://www.cfour.de>.
35. Valeev, F. E.; Sherrill, D. C. The diagonal Born-Oppenheimer correction beyond the Hartree-Fock approximation *J. Chem. Phys.* **2003**, *118*, 3921-3927.
36. Pfeiffer, F.; Rauhut, G.; Feller, D.; Peterson, K. A. Anharmonic zero point vibrational energies: Tipping the scales in accurate thermochemistry calculations. *J. Chem. Phys.* **2013**, *136*, 044311.
37. Frisch, M. J.; Trucks, G. W.; Schlegel, H. B.; Scuseria, G. E.; Robb, M. A.; Cheeseman, J. R.; Scalmani, G.; Barone, V.; Mennucci, B.; Petersson, G. A.; Nakatsuji, H.; Caricato, M.; Li, X.; Hratchian, H. P.; Izmaylov, A. F.; Bloino, J.; Zheng, G.; Sonnenberg, J. L.; Hada, M.; Ehara, M.; Toyota, K.; Fukuda, R.; Hasegawa, J.; Ishida, M.; Nakajima, T.; Honda, Y.; Kitao, O.; Nakai, H.; Vreven, T.; Montgomery, J. A., Jr.; Peralta, J. E.; Ogliaro, F.; Bearpark, M.; Heyd, J. J.; Brothers, E.; Kudin, K. N.; Staroverov, V. N.; Kobayashi, R.; Normand, J.; Raghavachari, K.; Rendell, A.; Burant, J. C.; Iyengar, S. S.; Tomasi, J.; Cossi, M.; Rega, N.; Millam, N. J.; Klene, M.; Knox, J. E.; Cross, J. B.; Bakken, V.; Adamo, C.; Jaramillo, J.; Gomperts, R.; Stratmann, R. E.; Yazyev, O.; Austin, A. J.; Cammi, R.; Pomelli, C.; Ochterski, J. W.; Martin, R. L.; Morokuma, K.; Zakrzewski, V. G.; Voth, G. A.; Salvador, P.; Dannenberg, J. J.; Dapprich, S.; Daniels, A. D.; Farkas, Ö.; Foresman, J. B.; Ortiz, J. V.; Cioslowski, J.; Fox, D. J. Gaussian 09, revision E.01; Gaussian, Inc.: Wallingford, CT, 2010.
38. Barone, V. Anharmonic vibrational properties by a fully automated second-order perturbative approach *J. Chem. Phys.* **2005**, *122*, 014108.
39. Helgaker, T.; Klopper, W. Basis-set convergence of correlated calculations on water *J. Chem. Phys.* **1997**, *106*, 9639-9646.

40. Schwenke, W, D. On one-electron basis set extrapolation of atomic and molecular correlation energies *Mol Phys.* **2012**, *110*, 2557-2567.
41. Martin, J.M.L. Ab initio total atomization energies of small molecules –towards the basis set limit *Chem. Phys. Letters.* **1996**, *259*, 669-678.
42. Hill, J, G.; Peterson, K, A.; G, Knizia, G.; Werner, H, J. Extrapolating MP2 and CCSD explicitly correlated correlation energies to the complete basis set limit with first and second row correlation consistent basis sets. *J. Chem. Phys.* **2009**, *131*, 194105.
43. Feller, D.; Bross, H, D.; Ruscic, B. Enthalpy of Formation of N₂H₄(Hydrazine) Revisited. *J. Phys. Chem. A*, **2017**, *121*, 6187-6198.
44. Feller, D. Estimating the intrinsic limit of the Feller-Peterson-Dixon composite approach when applied to adiabatic ionization potentials in atoms and small molecules. *J. Chem. Phys.*, **2017**, *147*, 034103.
45. Yan, C.; Kocevskaja, S.; Krasnoperov, N, L. Kinetics of the Reaction of CH₃O₂ Radicals with OH Studied over the 292–526 K Temperature Range. *J. Phys. Chem. A*, **2016**, *120*, 6111-6121.
46. Drougas, E Quantum mechanical studies of the CH₃O₂ + HO₂ reaction. *Comp and Theo Chem*, **2016**, *1093*, 98-103.
47. Assaf, E.; Sheps, L.; Whalley, L.; Heard, D.; Tomas, A.; Schoemaeker, C.; Fittschen, C. The Reaction between CH₃O₂ and OH Radicals: Product Yields and Atmospheric Implications. *Environ. Sci. Technol.* **2017**, *51*, 2170–2177.
48. Shallcross, D. E.; Leather, K. E.; Bacak, A.; Xiao, P.; Lee, E. P. F.; Ng, M.; Mok, D. K. W.; Dyke, J. M.; Hossaini, R.; Chipperfield, M. P.; et al. Reaction between CH₃O₂ and BrO radicals: A new source of upper troposphere lower stratosphere hydroxyl radicals. *J. Phys. Chem. A* **2015**, *119*, 4618–4632
49. Voronva, K.; Ervin, K.; Torma, G, K.; Hemberger,.; Bodi, A.; Gerber, T.; Osborn, L, D.; Sztaray, B. Radical Thermometers, Thermochemistry, and Photoelectron Spectra: A Photoelectron Photoion Coincidence Spectroscopy Study of the Methyl Peroxy Radical. *J. Phys. Chem. Letters.* **2018**, *9*, 534-539.

50. Meloni, G.; Zou, P.; Klippenstein, J, S.; Ahmed, M.; Leone, R, S.; Taatjes, A, C.; Osborn, D. Energy-Resolved Photoionization of Alkylperoxy Radicals and the Stability of Their Cations *J. Am. Chem. Soc.* **2006**, *128*, 13559-13567.
51. Osborn, D. L. Reaction Mechanisms on Multiwell Potential Energy Surfaces in Combustion (and Atmospheric) Chemistry. *Annu. Rev. Phys. Chem.* **2017**, *68*, 233–260.
52. Goldsmith, C, F.; Magoon, R, G; Green, H, W. Database of Small Molecule Thermochemistry for Combustion. *J. Phys. Chem. A* **2012**, *36*, 9033-9057.
53. Ruscic, B.; Active Thermochemical Tables: Sequential Bond Dissociation Enthalpies of Methane, Ethane, and Methanol and the Related Thermochemistry. *J. Phys. Chem. A* **2015**, *119*, 7810-7837.
54. Nguyen, L. T; McCarthy, C. M; Stanton, F, J.; Relatively Selective Production of the Simplest Criegee Intermediate in a CH₄/O₂ Electric Discharge: Kinetic Analysis of a Plausible Mechanism. *J. Phys. Chem. A.* **2015**, *28*, 7197-7204.
55. Slagle, I. R.; Gutman, D. J.; Kinetics of Polyatomic Free Radicals Produced by Laser Photolysis. 5. Study of the Equilibrium CH₃ + O₂ = CH₃O₂ between 421 and 538°C. *J. Am. Chem. Soc.* **1985**, *107*, 5342-5347.
56. Knyazev, V. D; Slagle, I. R; Thermochemistry of the R-O₂ Bond in Alkyl and Chloroalkyl Peroxy Radicals. *J. Phys. Chem. A* **1998**, *102*, 1770-1778.
57. Khachatryan, L. A.; Niazyan, O. M.; Mantashyan, A. A.; Vedeneev, V. I.; Teitel'boim, M. A.; Experimental Determination of the Equilibrium Constant of the Reaction CH₃ + O₂ = CH₃O₂ during the Gas-Phase Oxidation of Methane. *Int. J. Chem. Kinet.* **1982**, *14*, 1231-1241.
58. Schalley, C. A.; Schroeder, D.;Schwarz, H.; A neutralization-reionization mass spectrometric study of alkyl hydroperoxide cation radicals and four distinguishable [C,H₃,O₂]⁺ isomers. *International Journal of Mass Spectrometry and Ion Processes.* **1996**, *153*, 173-199.
59. Anglada, M, J.; Crehuet, R.; Costa-Martins, M.; Francisco, S, J.; Ruiz-Lopez, M.; The atmospheric oxidation of CH₃OOH by the OH radical: the effect of water vapor. *Phys. Chem. Chem. Phys.* **2017**, *19*, 12331-12342.

60. Harding, B. L.; Georgievskii, Y.; Klippenstein, J. S. Accurate Anharmonic Zero-Point Energies for Some Combustion-Related Species from Diffusion Monte Carlo. *J. Phys. Chem. A*. **2017**, 121, 4334-4340.
61. Watanabe, K.; Yachi, C.; Song, J. X.; Kakuyama, S.; Nishibe, M.; Jin, J. S. Atmospheric hydroperoxides measured over a rural site in central Japan during spring: helicopter-borne measurements. *J. Atmos. Chem.* **2017**, <https://doi.org/10.1007/s10874-017-9368-6>.
62. Zhang, X.; He, Z. S.; Chen, M. Z.; Zhao, Y.; Hua, W. Methyl hydroperoxide (CH₃OOH) in urban, suburban and rural atmosphere: ambient concentration, budget, and contribution to the atmospheric oxidizing capacity. *Atmos. Chem. Phys.* **2012**, 12, 8951-8962.
63. Bozzelli, W. J.; Wang, H. Thermochemical Properties ($\Delta_f H^\circ(298\text{ K})$, $S^\circ(298\text{ K})$, $C_p(T)$) and Bond Dissociation Energies for C1–C4 Normal Hydroperoxides and Peroxy Radicals. *J. Chem. Eng. Data*. **2016**, 61, 1836-1849.
64. Simmie, M. J.; Black, G.; Curran, J. H.; Hinde, P. J. Enthalpies of Formation and Bond Dissociation Energies of Lower Alkyl Hydroperoxides and Related Hydroperoxy and Alkoxy Radicals. *J. Phys. Chem. A*. **2008**, 5010-5016.
65. Matthews, J.; Sinha, A.; Francisco, S. J.; Unimolecular dissociation and thermochemistry of CH₃OOH. *J. Chem. Phys.* **2005**, 122, 221101.
66. Li, Y.-M.; Sun, Q.; Li, H.-Y.; Ge, M.-F.; Wang, D.-X.; Characterization and Activity of CH₃OOH and CH₃CH₂OOH - Study on a Photoelectron Spectroscopy. *Chin. J. Chem.* **2015**, 23, 993-996.
67. Faragó, E. P.; Szori, M.; Owen, M. C.; Fittschen, C.; Viskolcz, B.; Critical Evaluation of the Potential Energy Surface of the CH₃ + HO₂ Reaction System. *J. Chem. Phys.* **2015**, 054308/1-11.
68. Blanksby, S. J.; Ramond, T. M.; Davico, G. E.; Nimlos, M. R.; Kato, S.; Bierbaum, V. M.; Lineberger, W. C.; Ellison, G. B.; Okamura, M. Negative-Ion Photoelectron Spectroscopy, Gas-Phase Acidity, and Thermochemistry of the Peroxyl Radicals CH₃OO and CH₃CH₂OO. *J. Am. Chem. Soc.* **2001**, 123, 9585–9596.
69. Sullivan, N. E.; N, Bethan, N. M.; Photodissociation dynamics of the simplest alkyl peroxy radicals, CH₃OO and C₂H₅OO, at 248 nm. *J. Chem. Phys.* **2018**, 148, 044309.

70. Lightfoot, P. D.; Cox, R. A.; Crowley, J. N.; Destriau, M.; Hayman, G. D.; Jenkin, M. E.; Moortgat, G. K.; Zabel, F. Organic peroxy radicals: Kinetics, spectroscopy, *Atmos. Environ. A* **1992**, 26, 1805.
71. Tyndall, G. S.; Cox, R. A.; Granier C.; Lesclaux, G. K.; Moortgat G. K.; Pilling, M. J.; Ravishankara, A. R.; Wallington, T. J Atmospheric chemistry of small organic peroxy radicals *J. Geophys. Res.* **2001**, 26, 12157.
72. Just, G. M. P.; Rupper, P.; Miller, T. A.; Meerts, W. L High-resolution cavity ringdown spectroscopy of the jet-cooled ethyl peroxy radical $C_2H_5O_2$ *J. Chem. Phys.* **2009**, 131, 184303.
73. Carstensen, H. H.; Dean, A. M.; Deutschmann, O.; Rate constants for the H abstraction from alkanes by RO_2 radicals: A system study on the impact of R and R' *Proceedings of the Combustion Institute* **2007**, 31, 149-157.
74. Closser, K. D.; Vogelhuber, K. M.; Hsieh, S Vibrational-torsional excitation and direct overtone photodissociation of ethyl hydroperoxide at 5v OH *J. Phys. Chem. A* **2008**, 112, 1238-1244.
75. Stathis, E.C.; Egerton, A. C. Note on heats of formation of ethyl and propyl peroxides *Trans. Faraday. Soc.* **1940**, 36, 606.

SECTION

2. CONCLUSIONS

This work developed and applied a new highly-accurate and fully automated computational thermochemical scheme to the methyl and ethyl peroxy families of species. The results from this work were incorporated into the ATcT thermochemical database to update the related methyl species, and using the assembled computational and experimental results, provide information for the newly added ethyl species. This work would have not been possible without the development of an automated protocol to generate the enthalpies of formation. These computations require many individual steps and such a tedious process would have taken much longer and be prone to errors if conducted by hand. Several new strategies such as basis set extrapolation schemes and other approximations were tested in the course of this work, where again automation made them much easier to compute. Automation is key to making highly accurate computational thermochemistry more routine and accessible to non-specialists. The legacy of this project is a powerful set of codes usable by the broader community. As a variety of people apply these procedures to systems of interest to them, and the new data is added to the database, the database coverage and therefore its general usefulness will grow in community driven direction

APPENDIX A.

SUPPORTING INFORMATION FOR PAPER I

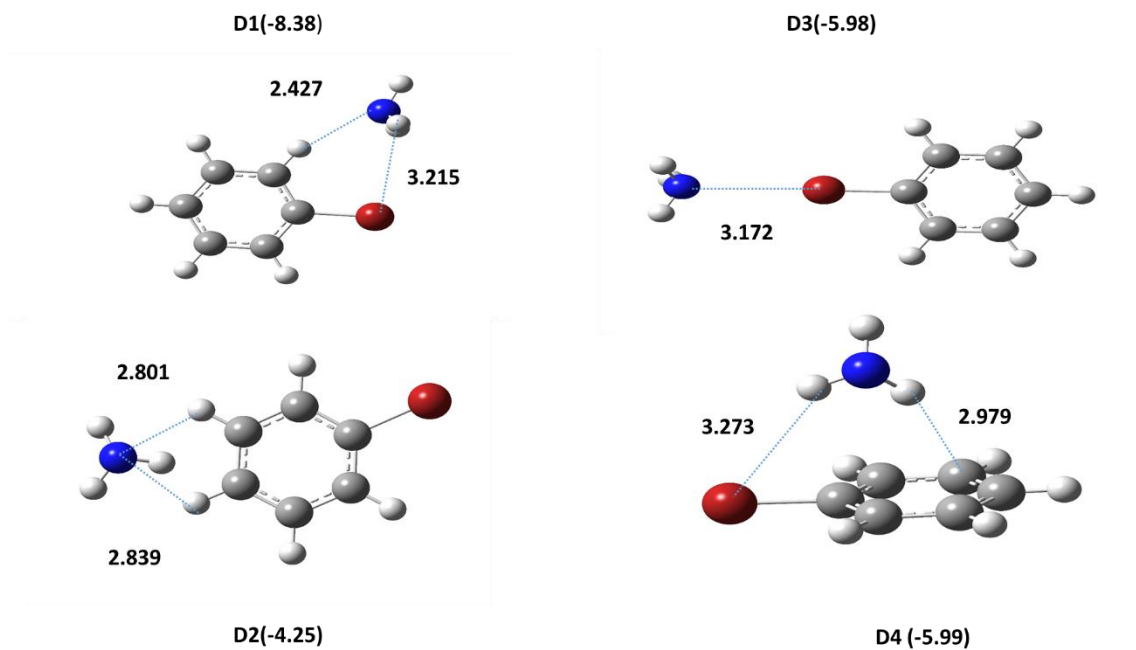


Figure A1. Ground state optimized geometries and ZPE-corrected binding energies (kJ/mol) for the PhBr-NH₃ 1:1 complexes. Geometries and ZPE corrections were calculated at the M06-2X/aug-cc-pVTZ level. To obtain binding energies, the ZPE corrections were added to single-point energies computed at the CCSD(T)-F12a/VDZ-F12 level.

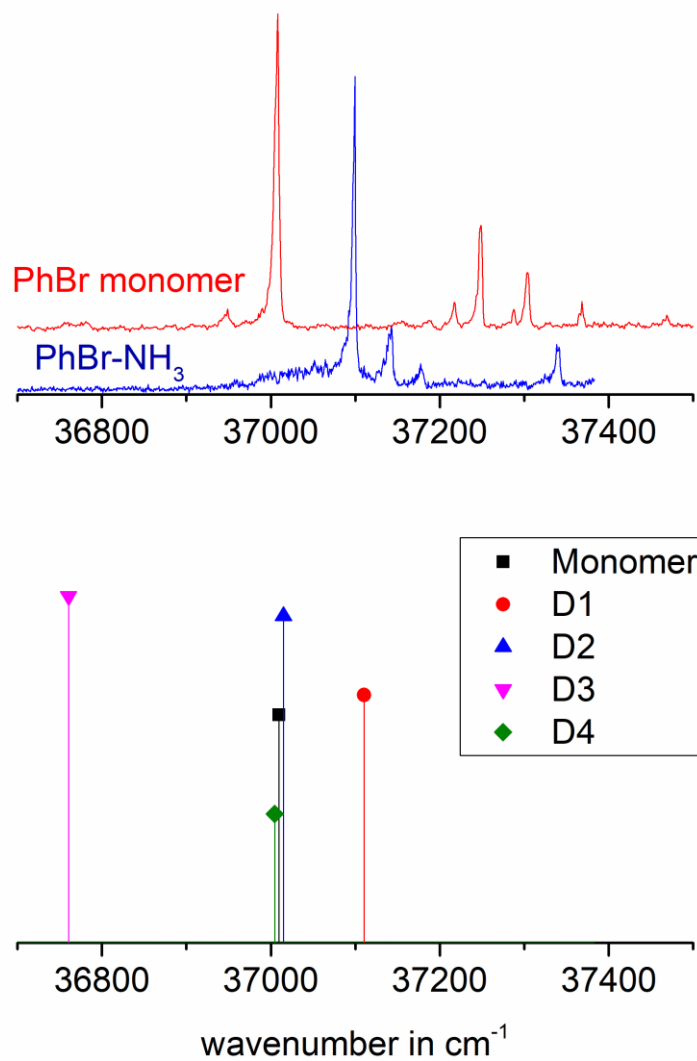


Figure A2. (a). R2PI spectra of PhBr monomer and the PhBr-NH₃ van der Waals cluster, obtained b=y monitoring the protonated aniline mass channel. (b). Calculated adiabatic transition energies of the PhBr monomer and four minimum energy dimer structures (D1-D4) from TDM06-2X/aug-cc-pVDZ optimizations of the S₀ and S₁ states, scaled to match the experimental value of the monomer absorption.

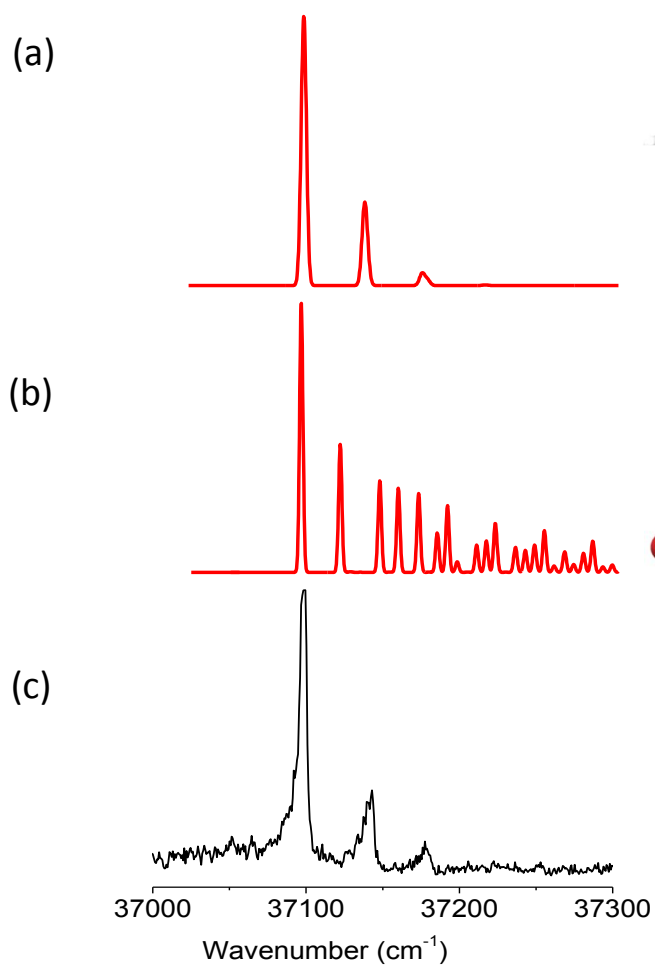


Figure A3. A comparison of the Franck-Condon simulations of the S1-S0 vibronic transitions in PhBr-NH₃ dimer for (a) σ -type (D1) isomer and (b) π -type (D4) isomer with experiment (c). The simulated stick spectra were convoluted with a Lorentzian linewidth of 5 cm⁻¹.

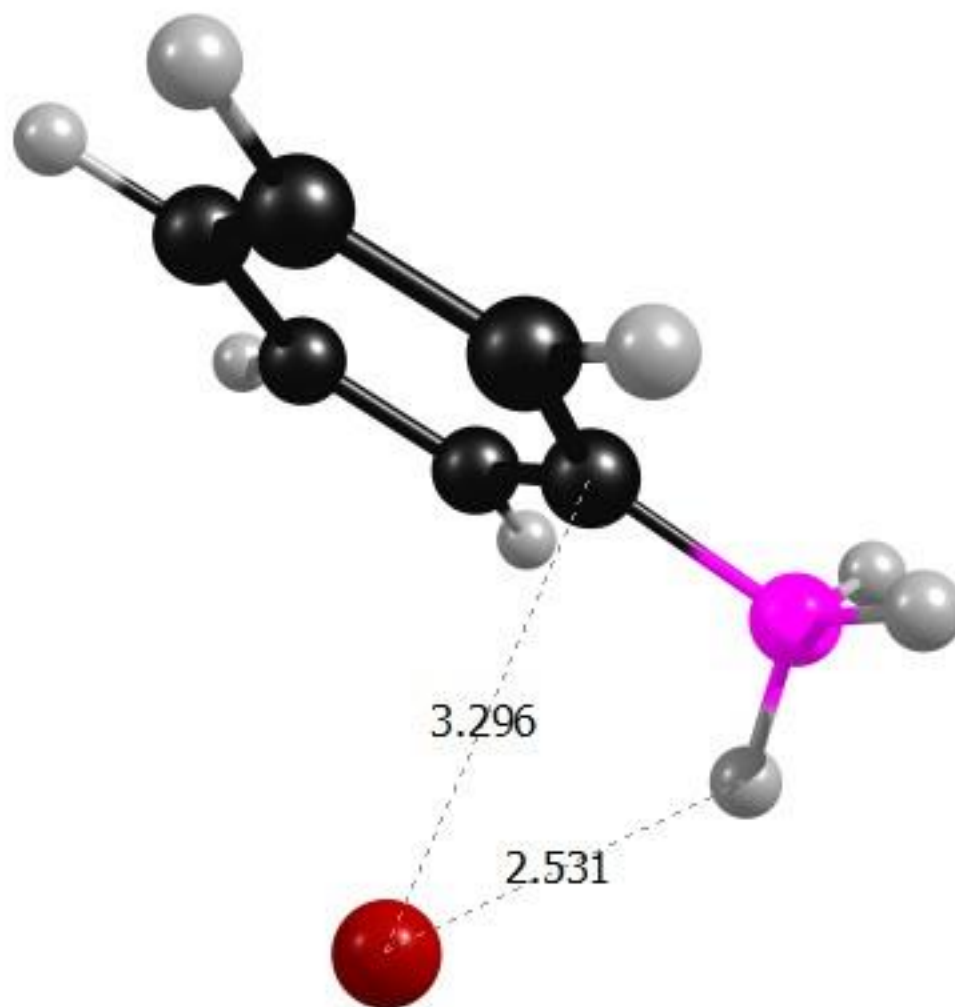


Figure A4. Optimized structure (M06-2X/aug-cc-pVTZ) of the (putative Wheland) intermediate formed following ionization of the PhBr-NH₃ dimer.

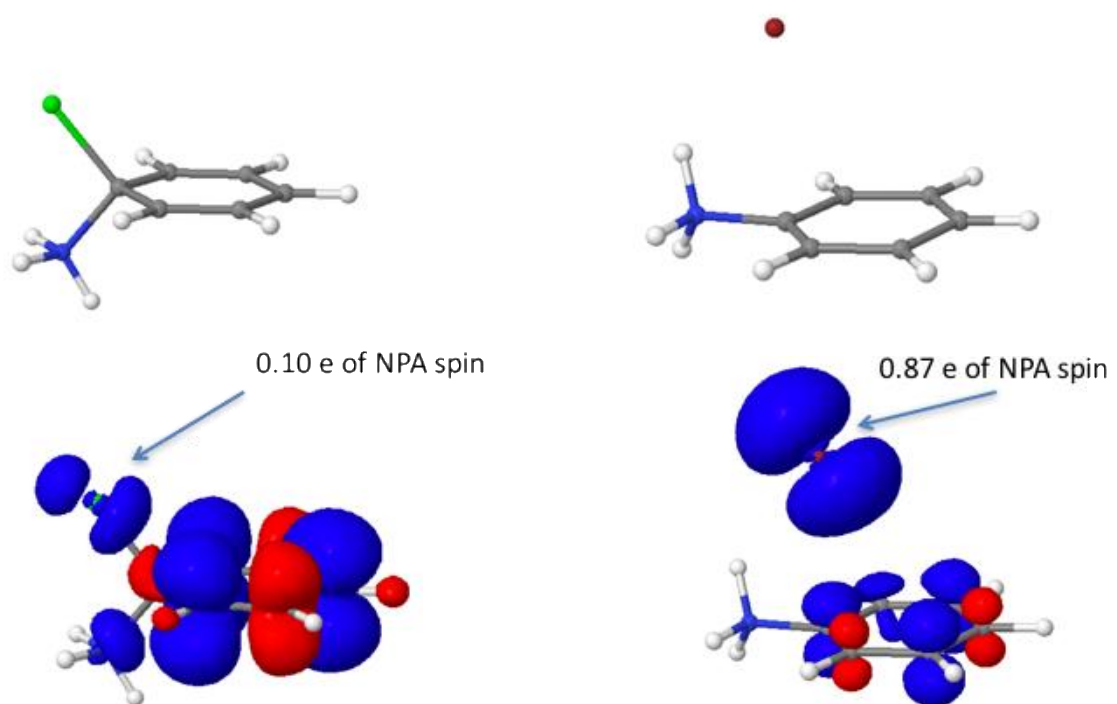


Figure A5. Comparison of calculated spin densities (B1LYP-40/6-31G*) of the intermediates found on the cation radical PES of ionized PhCl-NH₃ (left) and PhBr-NH₃ dimers.

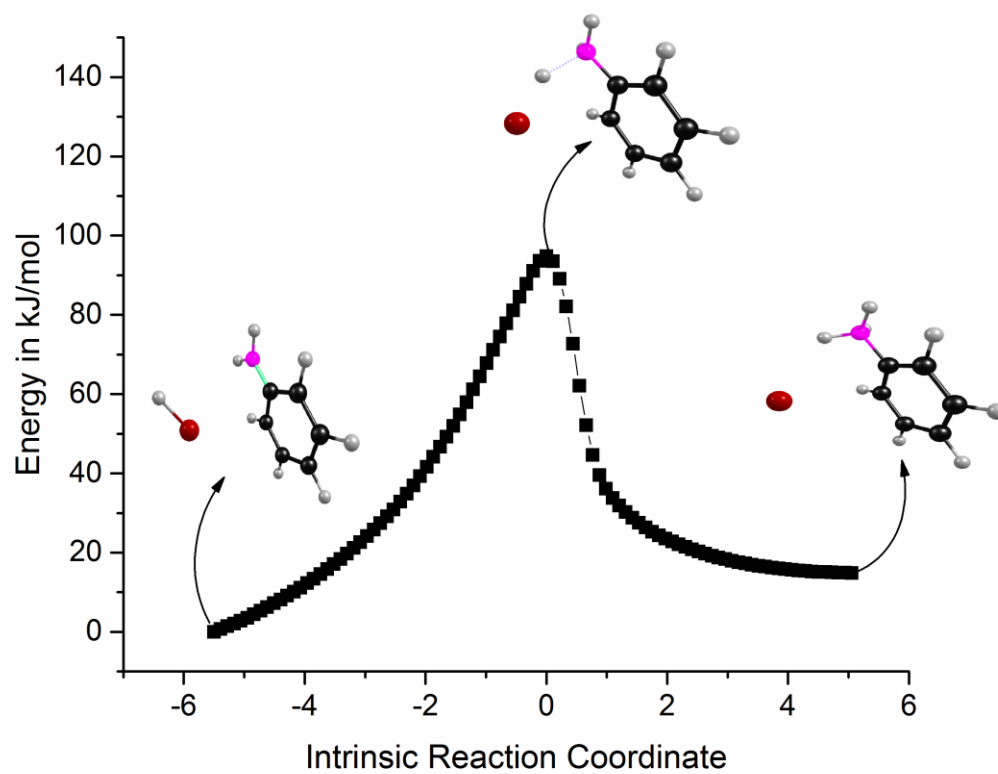


Figure A6. Intrinsic Reaction Coordinate calculation from the transition state to HBr elimination, calculated at the M06-2X/aug-cc-pVDZ level.

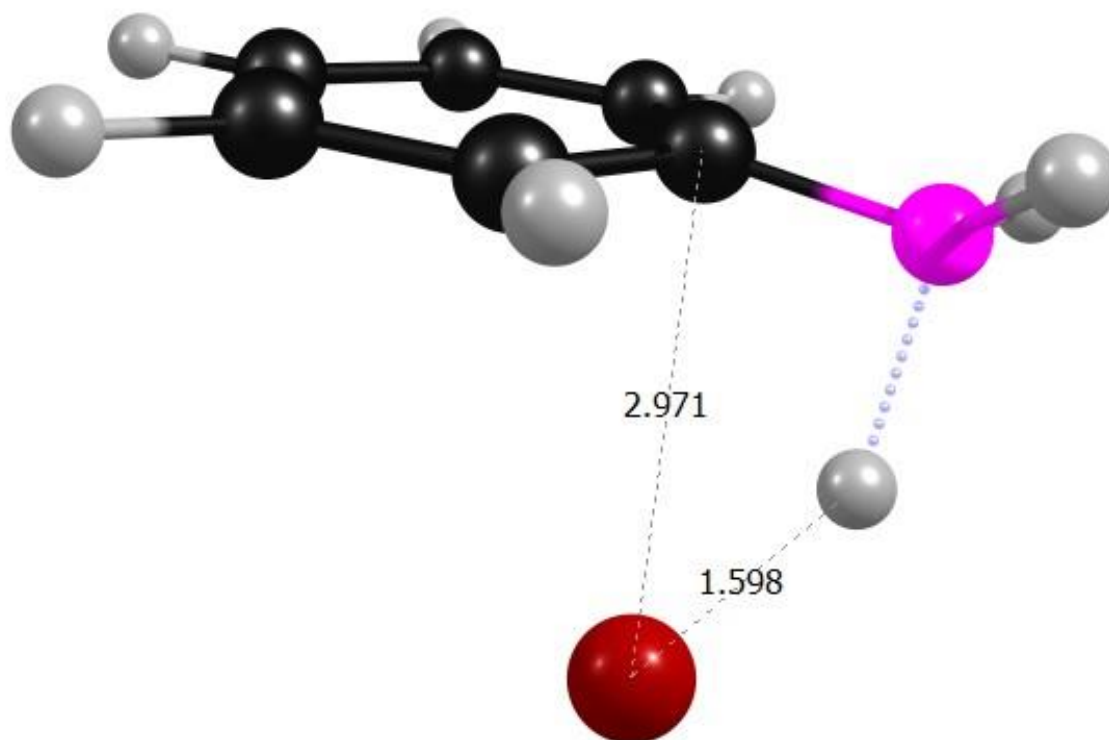


Figure A7. Optimized structure (M06-2X/aug-cc-pVTZ) of the transition state leading to HBr elimination from the intermediate formed following ionization of the PhBr-NH₃ dimer.

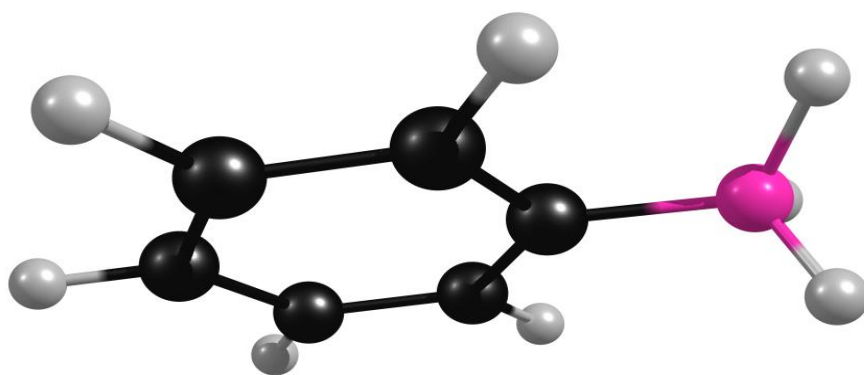


Figure A8. Optimized structure (CCSD/aug-cc-pVTZ) of the (putative Wheland) intermediate formed following ionization of the PhBr-NH₃ dimer.

Table A1. Parameters used in microcanonical TS calculations for the Br atom loss and HBr atom loss channels.

Adduct	$E_{\text{rel}} = 0 \text{ cm}^{-1}$			
Frequencies				
3605	3603	3293	3241	3234
3229	3217	3076	1664	1663
1659	1549	1477	1429	1396
1323	1228	1168	1155	1123
1104	1075	1030	1014	999
999	847	792	693	611
551	382	360	344	286
282	257	135	133	46
42	29			
TS: Br loss	$E_{\text{rel}} = 2706 \text{ cm}^{-1}$			
Frequencies				
3489	3470	3400	3241	3234
3224	3201	3200	1695	1658
1645	1643	1538	1515	1503
1363	1338	1206	1193	1187
1122	1078	1057	1037	1024
1009	1007	938	847	793
759	653	625	525	460
406	352	300	218	200
33				
TS: HBr loss	$E_{\text{rel}} = 5352 \text{ cm}^{-1}$			
Frequencies				
3590	3496	3242	3231	3224
3214	3211	1647	1627	1586
1546	1483	1389	1374	1317
1278	1200	1187	1138	1088
1051	1048	1028	1022	1001
962	920	864	819	765
688	620	547	507	454
413	394	333	221	83
66				

APPENDIX B.

SUPPORTING INFORMATION FOR PAPER II

Table B1. Electronic Energies of Atoms and Molecules

Procedure 1 ^a									
Species	$\Delta E(\text{HF})$	$\Delta E(\text{CCSD})$	$\Delta E(\text{T})$	$\Delta E(\text{Core})$	$\Delta E(\text{ZPVE})$	$\Delta E(\text{DBOC})$	$\Delta E(\text{Rel+SO})$	$\Delta E(\text{HOC})$	Total
C	-37.688688	-0.097907	-0.002669	-0.054632	0	0.00166	-0.015141	-0.000483	-37.857862
O	-74.812384	-0.18784	-0.004287	-0.061573	0	0.002366	-0.052692	-0.000356	-75.116767
H	-0.499999	0	0	0	0	0.000272	-0.000007	0	-0.499734
CH ₃ O ₂	-189.288871	-0.717198	-0.030443	-0.179842	0.042552	0.007081	-0.119062	-0.002226	-190.288009
CH ₃ O ₂ (+)	-188.943335	-0.684979	-0.029641	-0.179303	0.041398	0.007083	-0.119284	-0.002853	-189.91095
CH ₄ O ₂	-189.895143	-0.756237	-0.031559	-0.179998	0.054028	0.007248	-0.118909	-0.001843	-190.922455
CH ₃ O ₂ (-)	-189.278712	-0.763876	-0.035445	-0.17974	0.040701	0.00713	-0.118909	-0.001876	-190.330727
Procedure 2 ^a									
C	-37.688688	-0.097907	-0.002669	-0.054814	0	0.00166	-0.015141	-0.000545	-37.858107
H	-0.499999	0	0	0	0	0.000272	-0.000007	0	-0.499734
O	-74.812384	-0.18784	-0.004287	-0.062088	0	0.002366	-0.000671	-0.000427	-75.117353
CH ₃ O ₂	-189.288871	-0.717198	-0.030443	-0.181137	0.042552	0.007081	-0.119062	-0.002109	-190.289188
CH ₃ O ₂ (+)	-188.943335	-0.684979	-0.029641	-0.180589	0.041364	0.007083	-0.119284	-0.00281	-189.912192
CH ₃ O ₂ (-)	-189.278711	-0.763876	-0.035444	-0.18102	0.040701	0.00713	-0.118909	-0.001668	-190.331799
CH ₄ O ₂	-189.895143	-0.756237	-0.031559	-0.181286	0.054028	0.007248	-0.118909	-0.001669	-190.923568
Procedure 3 ^a									
C	-37.688688	-0.097907	-0.002669	-0.054632	0	0.00166	-0.015141	-0.000483	-37.857862
O	-74.812384	-0.18784	-0.004287	-0.061573	0	0.002366	-0.052692	-0.000356	-75.116767
H	-0.499999	0	0	0	0	0.000272	-0.000007	0	-0.499734
CH ₃ O ₂	-189.288818	-0.717228	-0.030461	-0.179838	0.042617	0.00708	-0.119062	-0.002232	-190.287944
CH ₃ O ₂ (+)	-188.94334	-0.684971	-0.029642	-0.179305	0.041501	0.007082	-0.119284	-0.002668	-189.910629
CH ₃ O ₂ (-)	-189.278675	-0.763896	-0.035458	-0.179738	0.040735	0.00713	-0.118909	-0.001876	-190.330689
CHO ₂ H	-189.895047	-0.75631	-0.031621	-0.179997	0.054155	0.007248	-0.11891	-0.001846	-190.922326
C ₂ H ₅ O ₂	-228.345178	-0.914513	-0.039035	-0.236353	0.070831	0.009187	-0.1337738	-0.002575	-229.591411
C ₂ H ₆ O ₂	-228.950969	-0.95365902	-0.040255	-0.236495	0.082385	0.009355	-0.1336231	-0.002221	-230.225483
C ₂ H ₅ O ₂ (-)	-228.335049	-0.961058	-0.044134	-0.236229	0.068662	0.009238	-0.133621	-0.002222	-229.634413

Table B1 Cont. Electronic Energies of Atoms and Molecules

	Procedure 4 ^a								
C	-37.688688	-0.097907	-0.002669	-0.054814	0	0.00166	-0.015141	-0.000545	-37.858107
O	-74.812384	-0.18784	-0.004287	-0.062088	0	0.002366	-0.000671	-0.000427	-75.117353
H	-0.499999	0	0	0	0	0.000272	-0.000007	0	-0.499734
CH ₃ O ₂	-189.288818	-0.717228	-0.0303928	-0.181125	0.042617	0.00708	-0.119062	-0.002115	-190.289114
CH ₃ O ₂ (+)	-188.94334	-0.684971	-0.029578	-0.180583	0.041501	0.007082	-0.119284	-0.002546	-189.911785
CH ₃ O ₂ (-)	-189.278675	-0.763896	-0.029642	-0.181012	0.040735	0.00713	-0.118909	-0.001668	-190.331755
CH ₄ O ₂	-189.895047	-0.75631	-0.031551	-0.181278	0.054155	0.007248	-0.11891	-0.001672	-190.923433
C ₂ H ₃ O ₂	-228.345178	-0.914513	-0.039035	-0.237857	0.070831	0.009187	-0.133773	-0.004367	-229.592759
C ₂ H ₆ O ₂	-228.950969	-0.95365902	-0.040255	-0.237993	0.082385	0.009355	-0.133623	-0.002012	-230.226772
C ₂ H ₅ O ₂ (-)	-228.335049	-0.961058	-0.044134	-0.237721	0.068662	0.009238	-0.133621	-0.001975	-229.635658

Table B2. Comparison of present results to previously reported thermochemistry data

Reaction	Determination	Value	$\Delta H(0K)$ kJ/mol ^a	$\Delta H(0K)$ kJ/mol Present work ^b	Reference
$CH_3OOH_{(g)} \rightarrow [CH_3OOH]_{(g)}^+$	Photoelectron	$\Delta H(0K) = 9.87 \pm 0.05$ eV	952.3 \pm 4.8	948.8	72
$CH_3OO_{(g)} \rightarrow [CH_3OO]_{(g)}^+$	Photoelectron	$\Delta H(0K) = 10.265 \pm 0.025$ eV	990.5 \pm 2.4		55
	Photoionization	$\Delta H(0K) = 10.33 \pm 0.05$ eV	996.7 \pm 4.8	991.8	56
	Theory CBS-APNO	$\Delta H(0K) = 10.21$ eV	985.1		56
$[CH_3OO]_{(g)}^- \rightarrow CH_3OO_{(g)}$	Photoelectron	$\Delta H(0K) = 1.161 \pm 0.005$ eV	112.02 \pm 0.48	112.99	74
$CH_3OO_{(g)} \rightarrow [CH_3]^+_{(g)} + O_{2(g)}$	Photoionization	$\Delta H(0K) = 11.16 \pm 0.05$ eV	1076.8 \pm 4.8	1077.4	56
	Photoionization	$\Delta H(0K) = 11.164 \pm 0.01$ eV	1077.2 \pm 1.0		55
$CH_3OO_{(g)} \rightarrow CH_3_{(g)} + O_{2(g)}$	Radical freezing	$\Delta G(750K) = 8.49 \pm 3.44$ kcal/mol	129 \pm 14		63
	3 rd law gas phase equilibrium	$\Delta G(753K) = 8.55 \pm 0.38$ kcal/mol	129.2 \pm 1.6		61
	2 nd law gas phase equilibrium	$\Delta H(753K) = 31.9 \pm 2.9$ kcal/mol	125 \pm 12		61
	3 rd law gas phase equilibrium	$\Delta G(753K) = 9.09 \pm 0.51$ kcal/mol	131.5 \pm 2.1	128.0	62
	2 nd law gas phase equilibrium	$\Delta H(753K) = 33.8 \pm 3.8$ kcal/mol	133 \pm 16		62
	Theory HEAT345(Q)	$\Delta H(0K) = 30.4$ kcal/mol	127.2		60
$CH_3OO_{(g)} + 5/2 H_{2(g)} \rightarrow CH_{4(g)} + 2H_2O_{(g)}$	Theory mHEAT345(Q)	$\Delta H(0K) = 30.75$ kcal/mol	128.7		60
	Theory	$\Delta H(0K) = -135.86$ kcal/mol	-568.4	-566.3	54
$[CH_3OO]_{(g)}^- + HCCH_{(g)} \rightarrow [CCH]_{(g)}^- + CH_3OOH_{(g)}$	Gas Phase Acidity	$\Delta G(298.15K) = 2.7 \pm 0.6$ kcal/mol	16.0 \pm 2.5	24.2	74
$CH_3OO_{(g)} \rightarrow C_{(g)} + 3H_{(g)} + 2O_{(g)}$	Theory HEAT345(Q)	$\Delta H(0K) = 1831.0$ kJ/mol	1831.0		60
	Theory ANL0	$\Delta H(0K) = 1831.3$ kJ/mol	1831.3	1831.3	17
$CH_3OO_{(g)} \rightarrow C_{(g)} + 3H_{(g)} + 2O_{(g)}$	Theory ANL0-F12	$\Delta H(0K) = 1833.1$ kJ/mol	1833.1		17
	Theory ANL0	$\Delta H(0K) = 2184.8$ kJ/mol	2184.8	2184.6	17
$CH_3OOH_{(g)} \rightarrow C_{(g)} + 4H_{(g)} + 2O_{(g)}$	Theory ANL0-F12	$\Delta H(0K) = 2186.7$ kJ/mol	2186.7		17
	Theory	$\Delta H(0K) = -22.48$ kcal/mol	-94.1	-92.7	54
$BrO_{(g)} + CH_3OO_{(g)} \rightarrow HOBr_{(g)} + CH_2OO_{(g)}$	Theory	$\Delta H(0K) = -22.48$ kcal/mol	-94.1	-92.7	54
$CH_3OOH_{(g)} \rightarrow CH_3O_{(g)} + OH_{(g)}$	Laser Induced Fluorescence	$\Delta H(0K) = 14775$ cm ⁻¹	176.7	181.4	71
	Laser Induced Fluorescence	$\Delta H(0K) = 15070$ cm ⁻¹	180.3		71
$CH_3OOH_{(g)} \rightarrow CH_3_{(g)} + HO_{2(g)}$	Theory CHEAT1	$\Delta H(0K) = 66.9 \pm 0.7$ kcal/mol	279.9	280.4	73

Table B3. Enthalpies of Formation of Ethylperoxy

Determination	Type	Enthalpy	T(K)	Ref
Knyazev and Slagle	Experiment	-27.19±10.14	298	55
Goldsmith, Magoon et al.	QCI Method	-5.00±3.77	0	51
	QCI Method	-20.92±3.77	298	
Blanksby <i>et al.</i>	CBS/APNO	-28.45±2.93	298	67
	Combination	-28.45±9.62		
Bozzelli and Wang	Average of theories	-25.90±3.85	298	63
Klippenstein, Harding <i>et al.</i>	ANL0	-6.1	0	13
	ANL0-F12	-5.9	0	
This work	Procedure 3	-5.56±2.19	0	
		-27.27±2.19	298	
	Procedure 4	-4.73±1.38	0	
		-26.45±1.38	298	

Table B4. Enthalpies of Formation of Ethyl Hydroperoxide

Determination	Type	Enthalpy	T(K)	Ref
Stathis and Egerton	Experiment	-188.28±50.21	298	75
Goldsmith, Magoon <i>et al.</i>	QCI Method	-142.80±3.77	0	51
	QCI Method	-161.08±3.77	298	
Blanksby <i>et al.</i>	CBS/APNO	-165.27±2.93	298	67
Wang and Bozzelli	Average of theories	-162.92±3.39	298	63
Klippenstein, Harding <i>et al.</i>	ANL0	-141.1	0	13
	ANL0-F12	-140	0	
This work	Procedure 3	-142.23±2.30	0	
		-167.09±2.30	298	
	Procedure 4	-141.25±1.39	0	
		-166.13±1.39	298	

Table B5. Enthalpies of Formation of Ethylperoxy anion

Determination	Type	Enthalpy	T(K)	Ref
Blanksby <i>et al.</i>	Experiment	114.432±0.386	0	67
	Combination	-142.88±9.63	298	67
This Work	Procedure 3	-118.46±2.67	0	
		-139.96±2.67	298	
	Procedure 4	-117.36±1.70	0	
		-138.86±1.70	298	

Table B6. Recommended Enthalpies of Formation from ATcT TN 1.122q kJ/mol

Species Name	Formula	ΔH_f (0K)	ΔH_f (298.15K)	Uncertainty
Methylperoxy	CH ₃ OO _(g)	22.05	12.60	± 0.36
Methoxyoxoniumylidene	CH ₃ OO ⁺ _(g)	1013.65	1004.82	± 0.67
Methylperoxy anion	CH ₃ OO ⁻ _(g)	-90.38	-100.52	± 0.48
Methyl hydroperoxide	CH ₃ OOH _(g)	-115.16	-127.99	± 0.49

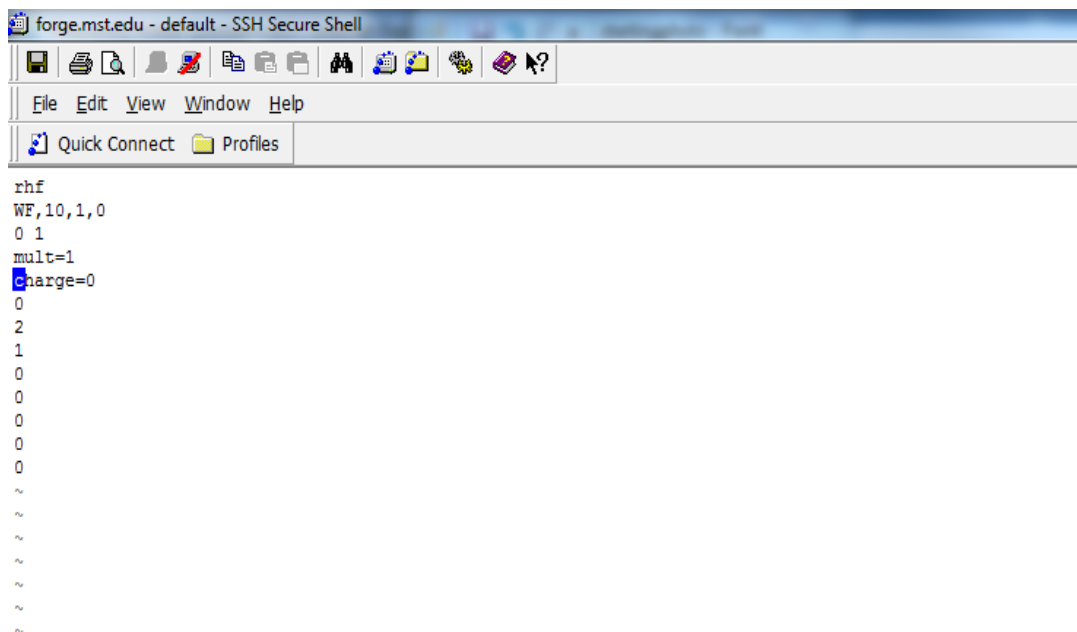
Table B7. Comparison of vibrational frequencies calculated at the VPT2 CCSD(T)-F12b/cc-pVTZ-F12 level with experiment.

CH ₃ O ₂ radical		CH ₃ O ₂ H		CH ₃ O ₂ anion	CH ₃ O ₂ cation
Calc.	Expt.	Calc.	Expt.	Calc.	
3029.25	3030.0	3600.47	x	2818.35	3109.46
3015.80	3020.0	2997.23	x	2779.38	3089.47
2962.00	2968.0	2967.92	2963.8	2700.93	2969.77
1454.35	1453.0	2906.39	x	1460.08	1482.41
1440.12	1440.0	1479.21	1478.1	1390.82	1401.45
1416.87	1414.0	1432.94	x	1381.09	1391.24
1185.87	1183.0	1421.07	x	1177.00	1352.88
1135.13	x	1321.56	1320.7	1143.15	1042.57
1120.39	1112.0	1179.50	x	1064.08	1002.11
915.12	902.0	1155.42	x	777.72	463.91
492.02	492.0	1026.25	x	425.33	308.76
136.19	x	831.07	x	264.6	104.33
5.61	RMSD	443.97	x		
		243.82	x		
		176.76	x		
		2.51	RMSD		

No known experimental data assigned for the anion and cation species

APPENDIX C

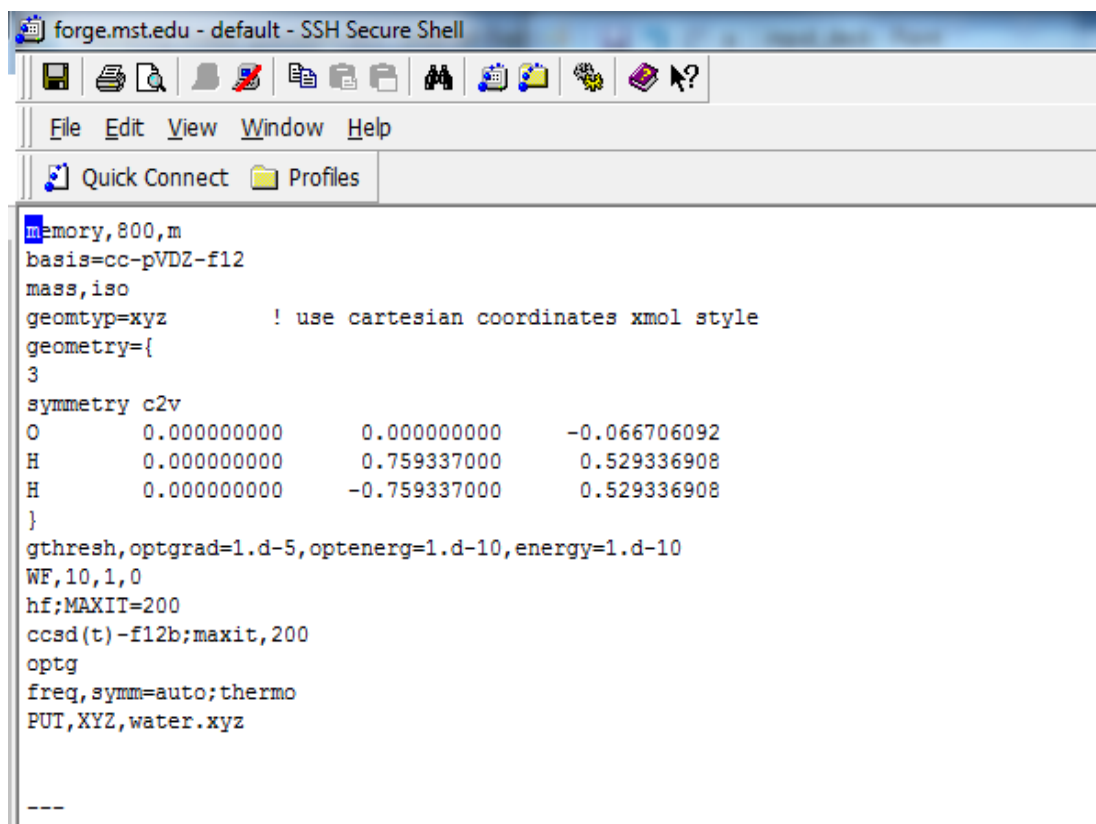
USER GUIDE TO EXATHERM V.1



The image shows a terminal window titled "forge.mst.edu - default - SSH Secure Shell". The window contains the following text:

```
rhf
WF,10,1,0
0 1
mult=1
charge=0
0
2
1
0
0
0
0
0
~
~
~
~
~
~
~
```

Figure C1. EXATHERM requires an input deck with wavefunction and atom numbers given. Here is water given as an example. The current version of the post processor supports C,H,O,N,F,B,Cl,Ar. Due to the fixed nature of the code it also requires MOLPRO WF input. The input deck must be saved as inputs.txt



```
forge.mst.edu - default - SSH Secure Shell
File Edit View Window Help
Quick Connect Profiles
memory,800,m
basis=cc-pVDZ-f12
mass,iso
geomtyp=xyz      ! use cartesian coordinates xmol style
geometry={
3
symmetry c2v
O      0.000000000    0.000000000    -0.066706092
H      0.000000000    0.759337000    0.529336908
H      0.000000000   -0.759337000    0.529336908
}
gthresh,optgrad=1.d-5,optenerg=1.d-10,energy=1.d-10
WF,10,1,0
hf;MAXIT=200
ccsd(t)-f12b;maxit,200
optg
freq,symm=auto;thermo
PUT,XYZ,water.xyz
---
```

Figure C2. The code requires an .xyz. One can start with a pre-optimized structure. It can also start with a geometry optimization and frequency computation. Using MOLPRO's .xyz writing ability it can then be fed to EXATHERM.


```

</input>
<!--
--></job><!--
--></molpro>
(base) [blwx97@login-44-0 water_tester_thesis]$ ls
3c2subnocore.sub  Gau-66744.inp      qznodk.sub      water_cc-pcvqz-f12.xml      water_cc-pcvtz_nocore-f12.xml      water_cc-pvtz-f12.xml      water_optfreq.log_
3c2sub.sub       h2o2.x            water_aug-cc-pvqz-dk.inp    water_cc-pcvqz_nocore-f12.inp    water_cc-pv5z-f12.inp      water.chk                water_optfreq.log_
3zsub.sub        inputs.txt        water_aug-cc-pvqz-dk.out    water_cc-pcvqz_nocore-f12.out    water_cc-pv5z-f12.out      water_mp2anharmonic_tz.com  water_optfreq.log_
4c2subnocore.sub  MRCC_CCSDparaT_cpvdz  water_aug-cc-pvqz-dk.xml    water_cc-pcvqz_nocore-f12.xml    water_cc-pv5z-f12.xml      water_mp2anharmonic_tz.log  water_optfreq.log_
4c2sub.sub       MRCC_CCSDparaT_cpvtz  water_aug-cc-pvqz_nodk.inp  water_cc-pcvtz-f12.inp        water_cc-pvqz-f12.inp      water_optfreq.inp         water_optfreq.log_
4zsub.sub        MRCC_CCSDT_cpvdz     water_aug-cc-pvqz_nodk.out  water_cc-pcvtz-f12.out        water_cc-pvqz-f12.out      water_optfreq.log         water_optfreq.log_
5zsub.sub        MRCC_CCSDT(Q)_cpvdz  water_aug-cc-pvqz_nodk.xml  water_cc-pcvtz-f12.xml        water_cc-pvqz-f12.xml      water_optfreq.log_001     water_optfreq.log_
DBOC             output            water_cc-pcvqz-f12.inp      water_cc-pcvtz_nocore-f12.inp    water_cc-pvtz-f12.inp      water_optfreq.log_002     water_optfreq.log_
g09sub.sub       qzdksub.sub       water_cc-pcvqz-f12.out      water_cc-pcvtz_nocore-f12.out    water_cc-pvtz-f12.out      water_optfreq.log_003     water_optfreq.log_
(base) [blwx97@login-44-0 water_tester_thesis]$

```

Figure C4. Once the optimization and frequency is done it will write input files for the computational scheme as well as submission files. It will also submit the submission to the queuing system and start the different computations.

```

(base) [blwx97@login-44-0 water_tester_thesis]$ ls
3c2subnocore.sub  h2o2.x            water_aug-cc-pvqz-dk.inp    water_cc-pcvqz_nocore-f12.inp    water_cc-pv5z-f12.inp    water.chk                water_optfreq.log_005  water_optfreq.log_014  water_optfreq.xml_006  water_optf
3zsub.sub         inputs.txt        water_aug-cc-pvqz-dk.out    water_cc-pcvqz_nocore-f12.out    water_cc-pv5z-f12.out    water_mp2anharmonic_tz.com  water_optfreq.log_006  water_optfreq.log_015  water_optfreq.xml_007  water.xyz
4zsub.sub         MRCC_CCSDparaT_cpvdz  water_aug-cc-pvqz-dk.xml    water_cc-pcvqz_nocore-f12.xml    water_cc-pv5z-f12.xml    water_mp2anharmonic_tz.log  water_optfreq.log_007  water_optfreq.out      water_optfreq.xml_008
4c2subnocore.sub  MRCC_CCSDparaT_cpvtz  water_aug-cc-pvqz_nodk.inp  water_cc-pcvtz-f12.inp          water_cc-pvqz-f12.inp    water_optfreq.inp         water_optfreq.log_008  water_optfreq.xml     water_optfreq.xml_009
4zsub.sub         MRCC_CCSDT_cpvdz     water_aug-cc-pvqz_nodk.out  water_cc-pcvtz-f12.out          water_cc-pvqz-f12.out    water_optfreq.log         water_optfreq.log_009  water_optfreq.xml_001  water_optfreq.xml_010
4zsub.sub         MRCC_CCSDT(Q)_cpvdz  water_aug-cc-pvqz_nodk.xml  water_cc-pcvtz-f12.xml          water_cc-pvqz-f12.xml    water_optfreq.log_001     water_optfreq.log_010  water_optfreq.xml_002  water_optfreq.xml_011
4zsub.sub         output            water_cc-pcvqz-f12.inp      water_cc-pcvtz_nocore-f12.inp    water_cc-pvtz-f12.inp    water_optfreq.log_002     water_optfreq.log_011  water_optfreq.xml_003  water_optfreq.xml_012
7BOC             qzdksub.sub       water_cc-pcvqz-f12.out      water_cc-pcvtz_nocore-f12.out    water_cc-pvtz-f12.out    water_optfreq.log_003     water_optfreq.log_012  water_optfreq.xml_004  water_optfreq.xml_013
j09sub.sub       qznodk.sub       water_cc-pcvqz-f12.xml      water_cc-pcvtz_nocore-f12.xml    water_cc-pvtz-f12.xml    water_optfreq.log_004     water_optfreq.log_013  water_optfreq.xml_005  water_optfreq.xml_014
(base) [blwx97@login-44-0 water_tester_thesis]$ schwenkmp2mrc:

```

Figure C5. Once the computations are done we can post process the results. Multiple postprocessing scripts for different extrapolations and schemes have been written. This particular script extrapolates CCSDT with the PVDZ and PVTZ basis sets. For the VPT2 term it uses MP2/PVTZ.

```

=====
***** OPTIMIZED - STRUCTURE *****
=====
OPTIMIZED GEOMETRY (xyz)
CCSD(T)-F12B/cc-pVDZ-F12 Energy:   -76.356754726685
O           0.0000000000           0.0000000000          -0.0612491192
H           0.0000000000           0.7570244894           0.5266084216
H           0.0000000000          -0.7570244894           0.5266084216

Initialization steps
=====
T1 Diag is 0.00882668
your T1 diagnostic is within acceptable tolerances
=====

***** POST - PROCESSING *****
=====
Sum of atomic energies -76.116820937589 Hartrees
Composite electronic energy -76.46652512407845702948 Hartrees
ATcT Enthalpy of Formation 0 k for atoms 678.912 kJ/mol
Total Atomization Energy is 918.14834162806943089974 kJ/mol
Enthalpy of Formation at 0 K is -239.23634162806943089974 kJ/mol
=====

***** TAE Breakdown *****
=====
Number of Carbons is 0
Number of Hydrogens is 2
Number of Oxygens is 1
Number of Nitrogens is 0
Number of Fluorines is 0
Number of Borons is 0
Number of Chlorines is 0
Number of Argons is 0

This next section gives the individual contributions of the component terms to the TAE.
This is important for both error analysis and determining if using a larger basis for CCSDT,
CCSDT(Q) and incorporating full quadruples is necessary.

HF contribution to TAE is 669.4520596685225 kJ/mol
CCSD-F12b contribution to TAE is 289.118163254784 kJ/mol
(T) contribution to TAE is 14.73856555951272539350kJ/mol
CVCBS TAE contribution is 1.59127153469881078597kJ/mol
Relativistic contribution to TAE is -1.122421041019kJ/mol
DBOC contribution to TAE is .5261496749kJ/mol
T/CBS TAE contribution is -.83830974796710527974kJ/mol
CCSDT(Q)/DZ contribution to TAE is 1.094557995783kJ/mol
ZPVE contribution to TAE is -55.5925404762kJ/mol
Spin-Orbit contribution to TAE is -.8191560 kJ/mol

Hartree % is .72913278749863415056
CCSD % is .31489264876535844363
(T) % is .01605248835213072412
CV/CBS % is .00173313119738053751
Relativistic % is -.00122248332881450535
DBOC % is .00057305519276659189
CCSDT/CBS % is -.00091304390582529006

```

Figure C6. Executing the submission script leads to the following output in a file called energies. It gives the optimized geometry. It also gives the Total Atomization Energy (TAE) as well as Enthalpy of Formation. Provided is a breakdown of the TAE as well as the fractional contribution. Below is the raw energies provided so one can test additional extrapolations or schemes for a given molecule.

BIBLIOGRAPHY

- [1] J. McCardle and D. Chester, "Measuring an Asynchronous Processor's Power and Noise," Synopsys User Group Conference (SNUG), Boston, 2001.
- [2] Pople, J. A.; Head-Gordon, M.; Fox, D. J.; Raghavachari, K.; Curtiss, L. A. Gaussian-1 theory: A general procedure for prediction of molecular energies. *J. Chem. Phys.* **1989**, 5622-29
- [3] Tajti, A.; Szalay, P. G.; Császár, A. G.; Kállay, M.; Gauss, J.; Valeev, E. F.; Flowers, B. A.; Vázquez, J.; Stanton, J. F. HEAT: High accuracy extrapolated ab initio thermochemistry. *J. Chem. Phys.* **2004**, 121, 11599–11613.
- [4] Martin, J. M. L.; Oliveira de G. Towards standard methods for benchmark quality ab initio thermochemistry-W1 and W2 theory. *J. Chem. Phys.* **1999**, 111, 1843.
- [5] Boese, A. D.; Oren, M.; Atasoylu, O.; Martin, J. M. L. W3 theory: Robust computational thermochemistry in the kJ/mol accuracy range. *J. Chem. Phys.* **2004**, 120, 4129.
- [6] Karton, A.; Rabinovich, E.; Martin, J. M. L. W4 thermochemistry for computational thermochemistry: In pursuit of confident sub-kJ/mol predictions. *J. Chem. Phys.* **2006**, 125, 144108.
- [7] Karton, A.; Sylvetsky, N.; Martin, J. M. L. W4-17: A Diverse and High-Confidence Dataset of Atomization Energies for Benchmarking High-Level Electronic Structure Methods. *J. Comp. Chem.* **2017**, 38, 2063-2075.
- [8] Kesharwani, M. K.; Brauer, B.; Martin, J. M. L. Frequency and Zero-Point Vibrational Energy Scale Factors for Double-Hybrid Density Functionals (and Other Selected Methods): can Anharmonic Force Fields Be Avoided?. *J. Phys. Chem. A* **2015**, 119, 1701-1714.
- [9] Harding, L. B.; Georgievskii, Y.; Klippenstein, S. J. Accurate Anharmonic Zero Point Energies for Some Combustion Related Species from Diffusion Monte Carlo. *J. Phys. Chem. A* 2017, 121, 4334–4340.
- [10] Klippenstein, S. J.; Harding, L. B.; Ruscic, B. Ab Initio Computations and Active Thermochemical Tables Hand in Hand: Heats of Formation of Core Combustion Species. *J. Phys. Chem. A* **2017**, 121, 6580–6602.
- [11] Valeev, F. E.; Sherrill, D. C. The diagonal Born-Oppenheimer correction beyond the Hartree-Fock approximation *J. Chem. Phys.* **2003**, 118, 3921-3927.

- [12] Adler, T. B.; Knizia, G.; Werner, H.-J. A Simple and efficient CCSD(T)-F12 approximation. *J. Chem. Phys.* **2007**, *127*, 221106-3.
- [13] Werner, H.-J.; Adler, T. B.; Manby, F. R., *J. Chem. Phys.* **2007**, *126*, 164102-18.
- [14] Pfeiffer, F.; Rauhut, G.; Feller, D.; Peterson, K, A. Anharmonic zero point vibrational energies: Tipping the scales in accurate thermochemistry calculations. *J. Chem. Phys.* **2013**, *136*, 044311.
- [15] Cox, J. D.; wagman, D. D.; Medvedev, V. A. *CODATA Key Values for Thermodynamics*; Hemisphere: New York, 1989.
- [16] Chase, M. W.; Davies, C. A.; Downey, J. R., Jr.; Frurip, D. J.; McDonald, R. A.; Syverud, A. N. *JANAF Thermochemical Tables*, 3rd ed.; *J. Phys. Chem. Ref. Data* **1985**, *14*, Suppl. 1. See also: Chase, M. W., Jr., Ed., *NIST-JANAF Thermochemical Tables*, 4th ed.; *J. Phys. Chem. Ref. Data*, **1998**, Monograph No. 9.
- [17] Gurvich, L. V.; Veyts, I. V.; Alcock, C. B. *Thermodynamic Properties of Individual Substances*, Vol. 1, Parts 1 and 2; Hemisphere: New York, 1989; Vol. 2, Parts 1 and 2; Hemisphere: New York, 1991; Vol. 3, Parts 1 and 2; Begell House: New York, 1996.
- [18] Ruscic, B.; Pinzon, R. E.; Morton, M. L.; Laszevski, G. V.; Bittner, S. J.; Nijssure, S. G.; Amin, K. A.; Minkoff, M.; Wagner, A. F. Introduction to Active Thermochemical Tables: Several “Key” Enthalpies of Formation Revisited†. *J. Phys. Chem. A* **2004**, *108*, 9979–9997.
- [19] Ruscic, B.; Pinzon, R. E.; von Laszewski, G.; Kodeboyina, D.; Burcat, A.; Leahy, D.; Montoya, D.; Wagner, A. F. Active Thermochemical Tables: Thermochemistry for the 21st Century. *J. Phys. Conf. Ser.* **2005**, *16*, 561–570.
- [20] Ruscic, B. Uncertainty Quantification in Thermochemistry, Benchmarking Electronic Structure Computations, and Active Thermochemical Tables. *Int. J. Quantum Chem.* **2014**, *114*, 1097– 1101.
- [21] Ruscic, B. Active Thermochemical Tables: Sequential Bond Dissociation Enthalpies of Methane, Ethane, and Methanol and the Related Thermochemistry. *J. Phys. Chem. A* **2015**, *119*, 7810–7837.
- [22] Vazquez, J.; Harding, M. E.; Gauss, J.; Stanton, J. F. High-Accuracy Extrapolated ab Initio Thermochemistry of the Propargyl Radical and the Singlet C₃H₂ Carbenes *J. Phys. Chem. A* **2009**, *113*, 12447.

VITA

Bradley Kenneth Welch received his B.S in chemistry at Saint Louis University in 2013. In 2015 he received the M.S. in chemistry from Saint Louis University under the supervision of Dr. Charles Kirkpatrick. Bradley then came to Missouri University of Science and Technology under the supervision of Dr. Richard Dawes. He received the Chancellors Fellowship and the DOE SCGSR fellowship while attending Missouri University of Science and Technology. He received the PhD in Chemistry in July 2019.